

AD-A033 925

RECOVERY OF GRAVITY ANOMALIES FROM GRIDDED GEOID HEIGHT 1/1

DATA(U) DEFENSE MAPPING AGENCY AEROSPACE CENTER ST

LOUIS AIR FORCE STATION MO M E SHULTZ ET AL. JUL 76

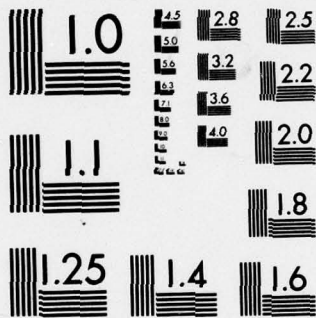
UNCLASSIFIED

DMAAC/TR-76-001

F/G 8/5

NL

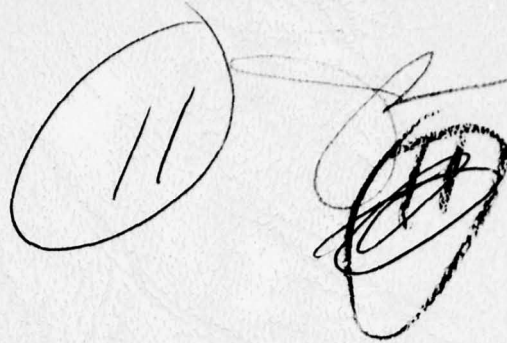




MICROCOPY RESOLUTION TEST CHART  
NATIONAL BUREAU OF STANDARDS-1963-A

ADA033925

DMAAC/TR-76-001



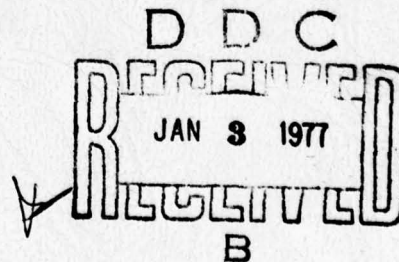
# RECOVERY OF GRAVITY ANOMALIES FROM GRIDDED GEOID HEIGHT DATA

JULY 1976



APPROVED FOR PUBLIC RELEASE;  
DISTRIBUTION UNLIMITED

DEFENSE MAPPING AGENCY  
AEROSPACE CENTER  
ST. LOUIS AIR FORCE STATION, MISSOURI 63118



DMAAC/TR-76-001

RECOVERY OF GRAVITY ANOMALIES  
FROM GRIDDED GEOID HEIGHT DATA

JULY 1976

Geophysical and Space Sciences Division  
Research Department

Approved for Public Release;  
Distribution Unlimited

DEFENSE MAPPING AGENCY

AEROSPACE CENTER

ST. LOUIS AFS, MISSOURI 63118

ACCESSION NO.	
NTIS	Write Section <input checked="" type="checkbox"/>
CRS	Diff Section <input type="checkbox"/>
UNANNOUNCED	<input type="checkbox"/>
JUSTIFICATION	
BY	
DISTRIBUTION / AVAILABILITY CODES	
Dist.	AVAIL. and or SPECIAL
A	

(See form 1473)



### ACKNOWLEDGEMENTS

This report represents the combined efforts of the following contributors from the Weapon Systems Support Branch: Messrs. Melvin E. Shultz, Robert M. Perlman, Joel B. Starkey, James M. Barth, Daniel J. Browning, and Roe R. Davenport. In addition, contributions were made by Messrs. Kenneth L. Brace and Egon J. Wetzker of the Geodetic and Geophysical Products Branch.

APPROVED FOR PUBLICATION	
<input type="checkbox"/> DISSEMINATE	DATE
<input type="checkbox"/> INTERNAL USE	DATE
APPROVED BY	
DATE	
CHIEF, WEAPON SYSTEMS SUPPORT BRANCH	
DATE	
CHIEF, GEODETIC AND GEOPHYSICAL PRODUCTS BRANCH	
DATE	

## PREFACE

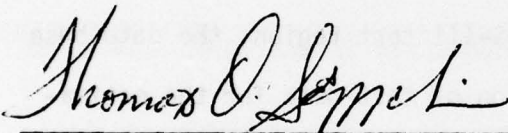
**GENERAL:** This publication is one of a series of reports on achievements related to the fields of mapping, charting and geodesy, and their related arts and sciences. Each report is written by a Defense Mapping Agency Aerospace Center scientist qualified by training and experience to contribute knowledge and technology to the selected subject. The Defense Mapping Agency Aerospace Center shall not be responsible for publishing revisions or for identifying the obsolescence of its technical publications.

**PURPOSE:** To contribute technical information to the field of geodesy by describing a method for estimating gravity anomalies from satellite derived geoid height data.

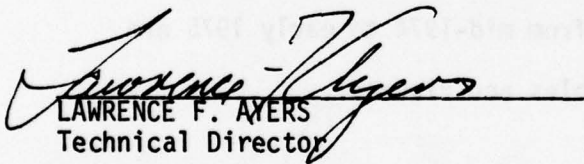
**REPRODUCTION:** This publication does not contain copyrighted material, nor is a copyright pending. Reproduction in whole or in part is permitted for any purpose of the United States Government.

**DISTRIBUTION:** Qualified requesters may obtain copies from the Defense Documentation Center, Cameron Station, Virginia 22314.

### REVIEWED



THOMAS O. SEPPELIN  
Chief, Research Department



LAWRENCE F. AYERS  
Technical Director

### APPROVED



JAMES H. ST. CLAIR, Colonel, USAF  
Director

# ABSTRACT

A gridded data base of geoid heights can be developed from GEOS-III satellite altimetry data. The derivation of two methods is discussed. A procedure for estimating gravity anomalies from the resulting geoid heights is described with simulations shown in tabular and graphic form. The report also discusses the computation of the calibration geoid for the GEOS-III test region, the data base from altimetry data and the simulation of test data for the estimation program. The method of localization for estimation and the methods of testing the computer program are given in some detail. Test results which were computed from mid-1974 to early 1975 are included along with supporting tables and figures.



## CONTENTS

	<u>Page</u>
ACKNOWLEDGEMENTS	ii
PREFACE	iii
ABSTRACT	iv
LIST OF ILLUSTRATIONS	vi
LIST OF TABLES	vii
I. INTRODUCTION	1
II. GRAVIMETRIC GEOID HEIGHTS	5
III. THE GRIDDED DATA BASE	9
A. Point Prediction Method	9
B. Profile Prediction Method	14
IV. ESTIMATION OF GRAVITY ANOMALIES	15
A. Stokes' Integral	15
B. Localization of Stokes' Integral Equation	17
C. Contributions of Distant Zones and High Harmonic Degrees to Computed Geoid Height	21
D. Effects of Errors in the Low Degree Component	23
E. Method of Estimating Anomalies	24
V. TEST DATA SIMULATION	27
VI. PROGRAM INPUT AND TEST RESULTS	31
VII. CONCLUSIONS	51
APPENDIX	53
REFERENCES	71



# ILLUSTRATIONS

<u>Figure</u>		<u>Page</u>
1	Geometry of The Geoid Height Measurement	3
2	Computation Scheme for Gravimetric Geoid Heights	6
3	Gravimetric Geoid Heights for the GEOS-III Calibration Test Region (meters)	7
4	Gridded Data Base	10
5	Stokes' Kernel Function with Low Degree Harmonics Removed	19
6	Expected Error in N Due to Exclusions of Distant Zones	22
7	GEOS-III Spherical Harmonic Model Test	30
8	Hypothetical Geoid Heights (n,m=2→141) (meters)	32
9	Hypothetical Gravity Anomalies (n,m=2→141) (mgal)	33
10	Amplitude Spectrum of 1° x 1° Point Gravity Anomalies ( $\Delta g$ )	40
11	Amplitude Spectrum of 1° x 1° Mean Gravity Anomalies ( $\Delta \bar{g}$ )	41
12	Amplitude Spectrum of 1° x 1° Estimated Gravity Anomalies ( $\Delta \hat{g}$ )	42
13	Amplitude Spectrum of 1° x 1° Estimation Errors ( $\Delta \hat{g} - \Delta g$ )	43
14	Amplitude Spectrum of 1° x 1° Estimation Errors ( $\Delta \bar{\hat{g}} - \Delta \bar{g}$ )	44
15	Effects of Random Error on Gravity Anomalies	49

# TABLES

<u>Table</u>		<u>Page</u>
1	1° x 1° POINT GRAVITY ANOMALIES FROM THE HYPOTHETICAL HIGH DEGREE FIELD $n,m = 13 \rightarrow 141$ ( $\Delta g$ , mgal)	34
2	1° x 1° SMOOTHED MEAN GRAVITY ANOMALIES FROM THE HYPOTHETICAL HIGH DEGREE FIELD $n,m = 13 \rightarrow 141$ ( $\overline{\Delta g}$ , mgal)	35
3	1° x 1° ESTIMATED GRAVITY ANOMALIES FROM GRIDDED GEOID USING THE HYPOTHETICAL HIGH DEGREE FIELD $n,m = 13 \rightarrow 141$ ( $\Delta \tilde{g}$ , mgal)	36
4	ERROR OF ESTIMATION ( $\Delta \tilde{g} - \Delta g$ ) FOR 1° x 1° POINT VALUES (mgal)	38
5	ERROR OF ESTIMATION ( $\Delta \tilde{g} - \overline{\Delta g}$ ) FOR 1° x 1° MEAN VALUES (mgal)	39
6	ERROR OF ESTIMATION ( $\hat{\Delta g} - \overline{\Delta g}$ ) FOR 1° x 1° MEAN VALUES FROM A GEOID WITH A RANDOM ERROR OF ONE METER	46
7	ERROR OF ESTIMATION ( $\hat{\hat{\Delta g}} - \overline{\Delta g}$ ) FOR 1° x 1° MEAN VALUES FROM A GEOID WITH A BIAS ERROR OF ONE METER	47
8	ITERATIVE IMPROVEMENT (36 1° x 1° SQUARES)	48

## I. INTRODUCTION

Prior to the launching of the first artificial satellite in 1957, the best approximation for the gravitational potential field of the earth was a spherical harmonic series to degree and order four obtained from studies of the moon's orbit and gravity observations at a few scattered land stations. Extensive satellite tracking data has made it possible to analyze orbital perturbations for a more detailed representation of the potential field. In recent years technical developments in improved satellite tracking and advances in missile weapon systems have increased the need for a more accurate representation of the potential field to higher harmonic degree and order. The incorporation of orbital data with an increasing number of gravity observations on land has allowed approximation of the potential field to degree and order twenty with several zonal and tesseral coefficients beyond that level. The models developed by several investigators during the last few years are fairly consistent to degree and order twelve. Usually, the lower degree harmonics are based on orbital data and the higher degree harmonics are developed from surface observations. Development of harmonic series to higher degree and order requires more detailed knowledge of the gravity field over the entire surface of the earth. Gravity data, particularly ocean gravity data, is generally not adequate outside North America.

The National Aeronautics and Space Administration (NASA) included a radar altimeter in the Geodynamics Experimental Ocean



Satellite (GEOS-III), launched 9 April 1975. The purpose of the altimeter is to measure the ocean surface topography in order to obtain a detailed representation of the geoid for the ocean regions. Geoid heights, deflections of the vertical, gravity anomalies and the gravitational potential are related in such a way that observations which are adequate for computing mean geoid heights are also sufficient for computing mean values of the other geodetic parameters. Principal investigators were selected by NASA to analyze and evaluate the data collected from the various experiments on board the satellite.

As a user of gravity information, DoD has developed a separate exploitation plan [1] to utilize GEOS-III altimetry data for geoid, deflection of the vertical and mean gravity anomaly information. As a part of this plan, the Naval Research Laboratory (NRL) corrects the altimetry data for tides, winds and ocean currents. The Naval Surface Weapons Center, Dahlgren Laboratory (NSWC DL) computes the corrected heights of the satellite above the geoid, along track geoid heights, geocentric radius of the satellite position and the ellipsoidal radius of the suborbital point (Figure 1).

This data is then provided to the Defense Mapping Agency Aerospace Center (DMAAC) for development of a gridded data base of estimated  $1^\circ \times 1^\circ$  and  $5^\circ \times 5^\circ$  mean geoid heights and gravity anomalies. This data, when combined with mean anomalies from surface gravity data and satellite orbital analysis, will be used to derive an improved earth gravitational model.



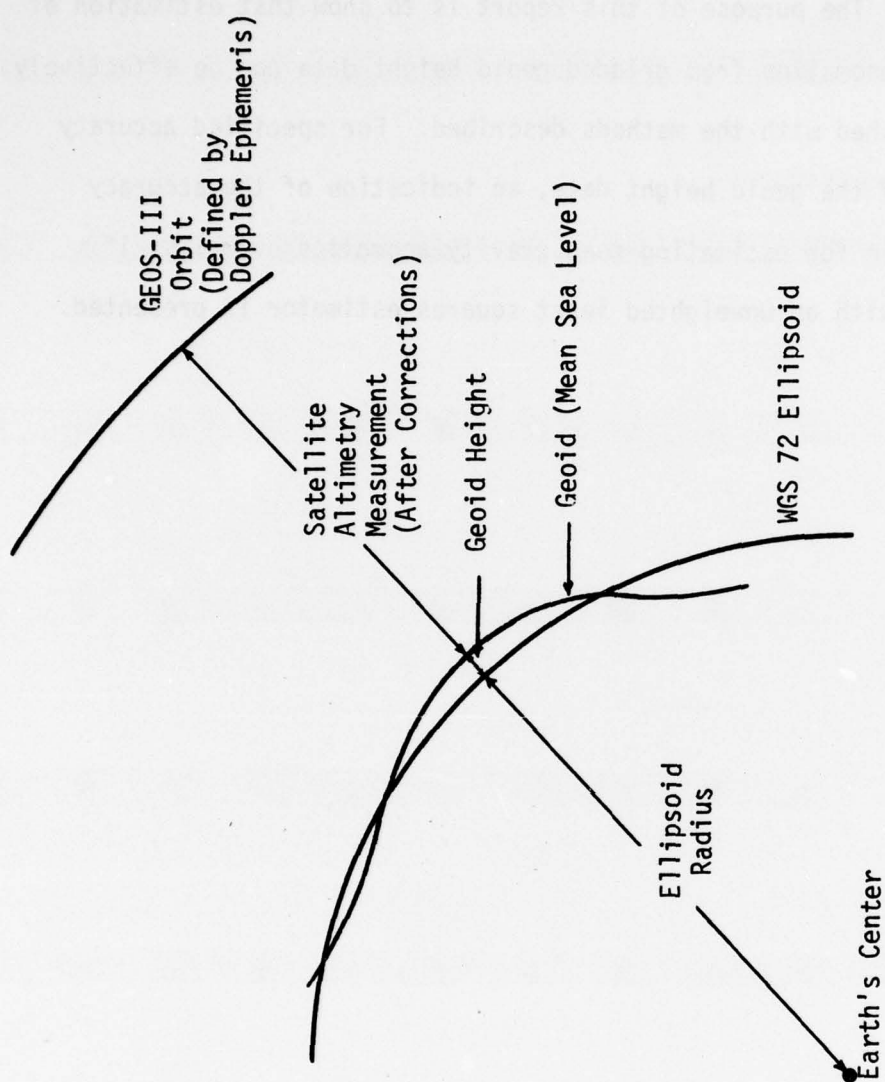


Figure 1. Geometry of the Geoid Height Measurement.

The purpose of this report is to show that estimation of gravity anomalies from gridded geoid height data can be effectively accomplished with the methods described. For specified accuracy levels of the geoid height data, an indication of the accuracy attainable for estimating mean gravity anomalies over  $1^\circ \times 1^\circ$  squares with an unweighted least squares estimator is presented.

## II. GRAVIMETRIC GEOID HEIGHTS

To provide a standard for comparison of satellite derived geoid heights, DMAAC computed gravimetric geoid heights over a region of the North Atlantic Ocean designated for GEOS-III calibration. The calculation required a worldwide integration of 5' x 5', 15' x 15', 1° x 1° and 5° x 5° elements, (Figure 2).

The mean free air gravity anomalies and their accuracies for the test region are stored on magnetic tapes in the DoD Gravity Library. These tapes are continually updated. Surface point values are not available for all the required 5' x 5' elements. Therefore, interim values have been obtained for the remaining elements by least squares prediction. The interim values constitute about 50 percent of all the required mean 5' x 5' gravity anomalies in the calibration area. The 15' x 15' and 1° x 1° values in the test region are means of 5' x 5' elements. The values for the worldwide array of 5° x 5° elements are averages of 1° x 1° elements obtained from observed data, geophysical correlation, extrapolation, etc.

Values for all 5° x 5° elements are referenced to the World Geodetic System 1972 (WGS 72) [2]. The anomaly data referenced to the WGS 72 gravity formula was used to compute the geoid heights at the centers of the 1° x 1° surface elements in the calibration region. A contour plot of these geoid heights is shown in Figure 3. Computations are being performed to expand the calibration region to include all of the North Atlantic to 65°N, the limit of GEOS-III coverage.

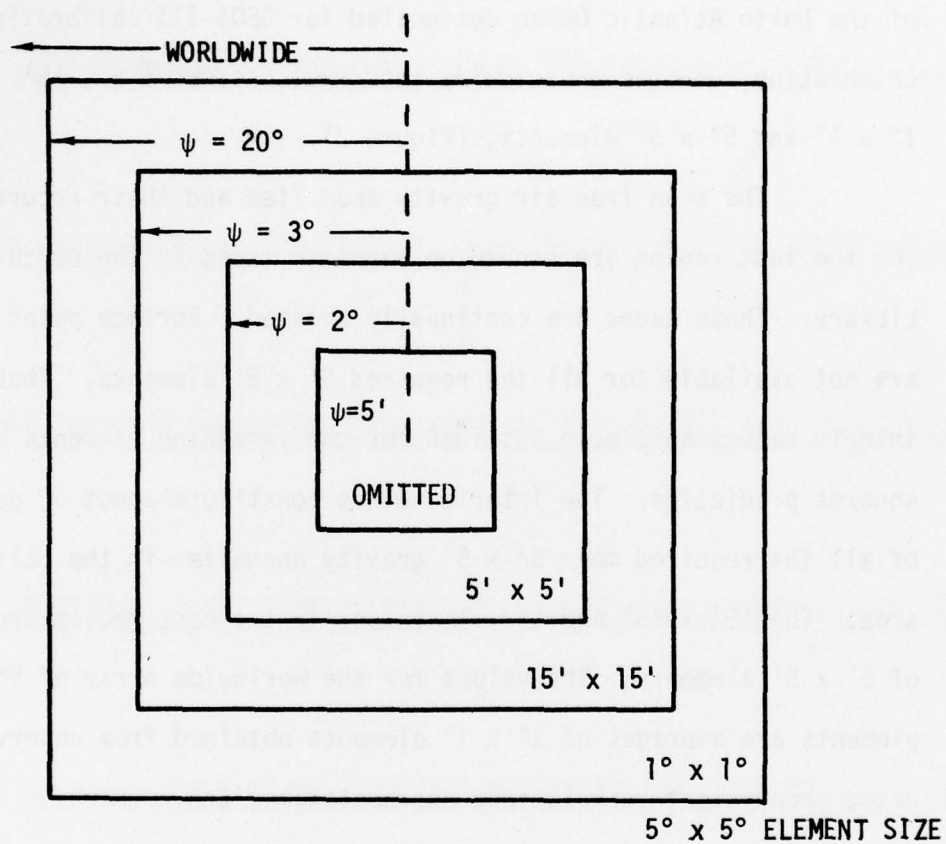


Figure 2. Computation Scheme for Gravimetric Geoid Heights.



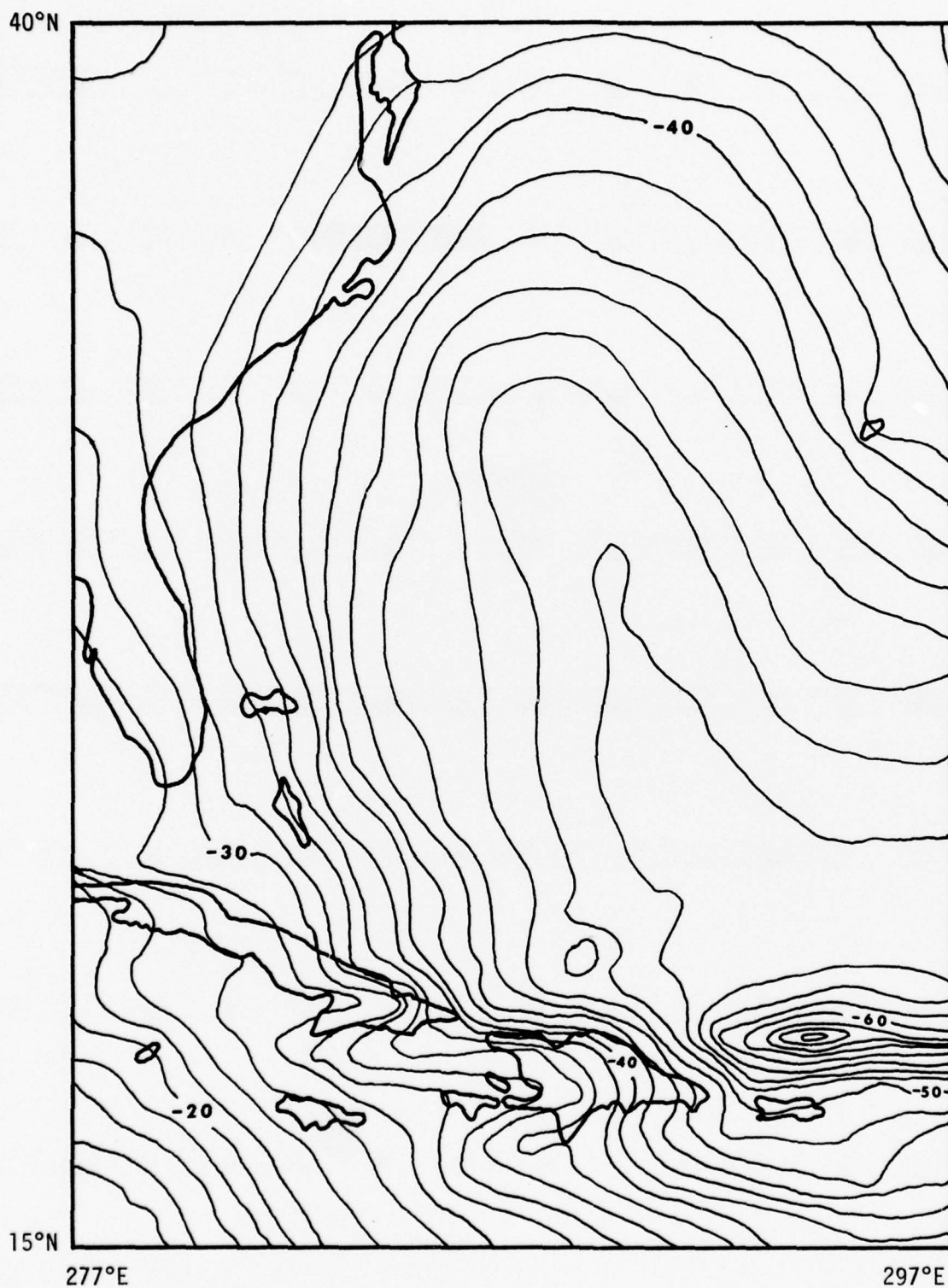


Figure 3. Gravimetric Geoid Heights for GEOS-III Calibration Test Region (meters).

### III. THE GRIDDED DATA BASE

The gridded data base consists of geoid heights and corresponding error variances estimated at the centers of  $1^\circ \times 1^\circ$  elements from GEOS-III data (Figure 4). The geoid height observations are regarded as the sum of a stochastic signal (true geoid height) and a stochastic noise (error). This section discusses two methods for obtaining the gridded geoid height data base: point prediction and profile prediction.

#### A. Point Prediction Method

The centered  $1^\circ \times 1^\circ$  values in the gridded data base are estimated by Wiener filtering and prediction which is a discrete least squares estimator [3]. It is assumed that the estimator  $\tilde{N}_p$  at a point P is a linear function of a set of observations  $N_i$  with prediction coefficients  $\alpha_{pi}$  such that

$$\tilde{N}_p = \alpha_{p1} N_1 + \alpha_{p2} N_2 + \dots + \alpha_{pn} N_n = \sum_{i=1}^n \alpha_{pi} N_i. \quad (1)$$

The prediction coefficients  $\alpha_{pi}$  depend on the geoid height autocovariance function and the positions of the n observation points relative to the calculation point P. The best estimates of the coefficients (from observed data) are obtained by minimizing the mean square error of prediction. If  $N_p$  is the true value of N at point P and  $\epsilon_p$  is the error of prediction, then

$$\epsilon_p = N_p - \tilde{N}_p = N_p - \sum_{i=1}^n \alpha_{pi} N_i, \quad (2)$$



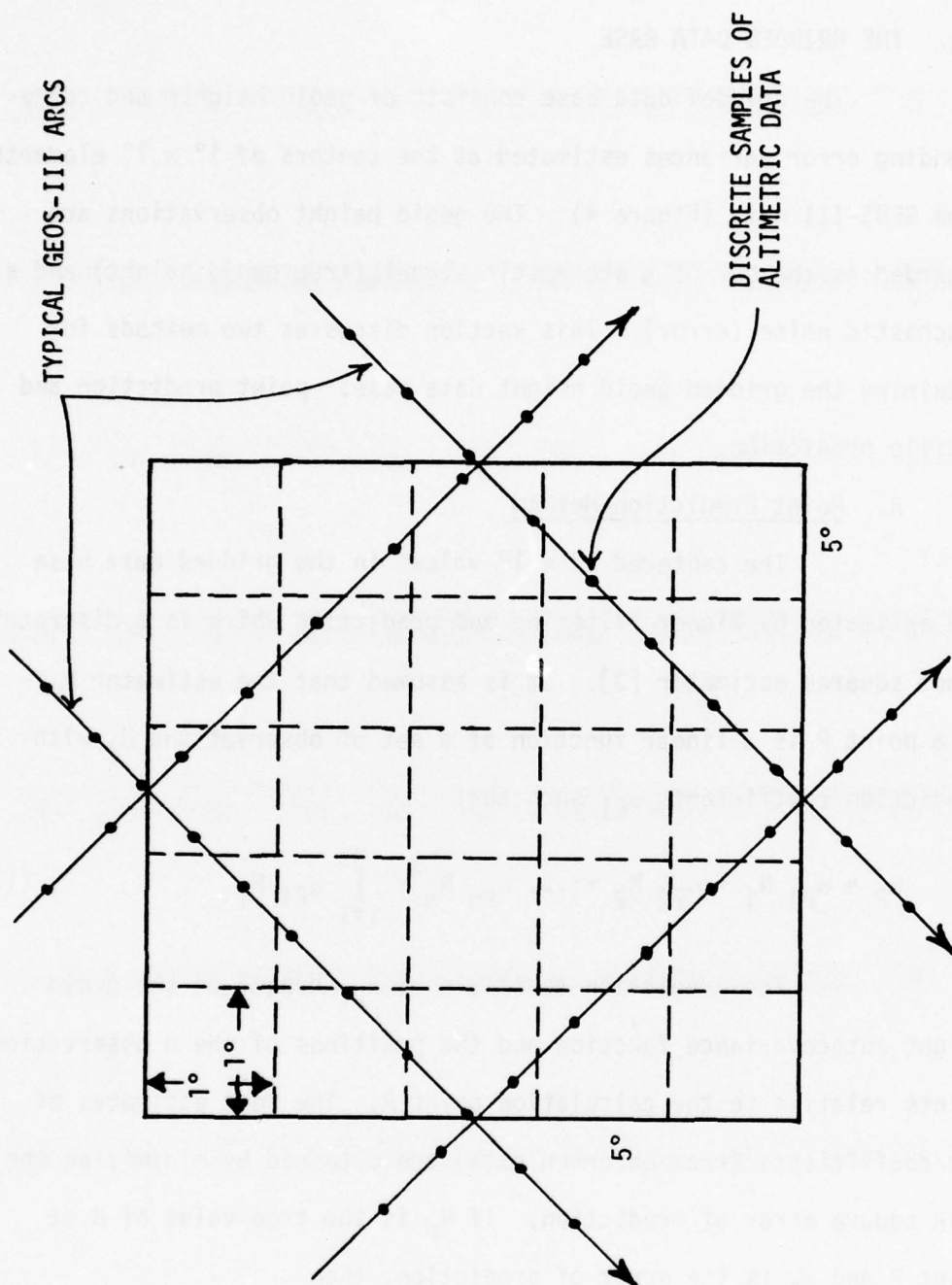


Figure 4. Gridded Data Base.



$$\epsilon_p^2 = (N_p - \sum_{i=1}^n \alpha_{pi} N_i)(N_p - \sum_{i=1}^n \alpha_{pi} N_i), \quad (3)$$

and

$$\epsilon_p^2 = N_p^2 - 2 \sum_{i=1}^n \alpha_{pi} N_p N_i + \sum_{i=1}^n \sum_{k=1}^n \alpha_{pi} \alpha_{pk} N_i N_k. \quad (4)$$

The geoid height covariances are estimated by averaging over the region of interest,

$M\{N_i N_k\} = C_{ik}$  = the covariance between the observed geoid heights at points  $i$  and  $k$ ,

$M\{N_p N_i\} = C_{pi}$  = the covariance between the geoid heights at the computation point  $P$  and the observed point  $i$ ,

$M\{N_p^2\} = C_0$  = the variance of the geoid height.

The mean square error of prediction of the geoid height at point  $P$  is

$$M\{\epsilon_p^2\} = m_p^2 = C_0 - 2 \sum_{i=1}^n \alpha_{pi} C_{pi} + \sum_{i=1}^n \sum_{k=1}^n \alpha_{pi} \alpha_{pk} C_{ik}. \quad (5)$$

The mean square prediction error is minimized by setting the derivative with respect to  $\alpha_{pi}$  to zero and solving for the coefficients.

Thus,

$$\frac{\partial m_p^2}{\partial \alpha_{pi}} = -2 C_{pi} + 2 \sum_{k=1}^n \alpha_{pk} C_{ik} = 0 \quad (i=1, 2 \dots n), \quad (6)$$

which reduces to a system of  $n$  linear equations

$$\sum_{k=1}^n C_{ik} \alpha_{pk} = C_{pi}, \quad (7)$$

with  $\alpha_{pk}$  as unknown coefficients. The solution for the coefficients is

$$\alpha_{pk} = \sum_{i=1}^n C_{ik}^{-1} C_{pi}. \quad (8)$$



Then the predicted geoid height becomes

$$\tilde{N}_p = \sum_{k=1}^n \alpha_{pk} N_k = \sum_{i=1}^n \sum_{k=1}^n C_{ik}^{-1} C_{pi} N_k, \quad (9)$$

which in matrix form is

$$\tilde{N}_p = (C_{p1}, C_{p2} \dots C_{pn}) \begin{bmatrix} C_{11} & C_{12} & \dots & C_{1n} \\ C_{21} & C_{22} & \dots & C_{2n} \\ \cdot & \cdot & & \cdot \\ \cdot & \cdot & & \cdot \\ C_{n1} & C_{n2} & & C_{nn} \end{bmatrix}^{-1} \begin{bmatrix} N_1 \\ N_2 \\ \cdot \\ \cdot \\ N_n \end{bmatrix}, \quad (10)$$

where  $N_1, N_2, \dots, N_n$  are the observed geoid heights.

The error variance of the least squares predictor is calculated by inserting the coefficients (8) into the error equation (5) which becomes

$$m_p^2 = \sigma_p^2 = C_0 - 2 \sum_{i=1}^n \sum_{k=1}^n C_{ik}^{-1} C_{pi} C_{pk} + \sum_i \sum_k \sum_j \sum_l C_{ik}^{-1} C_{pi} C_{jl}^{-1} C_{pj} C_{kl}. \quad (11)$$

with the subscripts  $j$  and  $l$  representing the same set of observed values as  $i$  and  $k$ .

Since

$$\sum_l C_{jl}^{-1} C_{kl} = \begin{cases} 1 & \text{if } j=k, \\ 0 & \text{if } j \neq k, \end{cases}$$

the error equation becomes

$$m^2_P = C_0 - \sum_{i=1}^n \sum_{k=1}^n C_{ik}^{-1} C_{Pi} C_{Pk}. \quad (12)$$

In matrix form this is

$$m^2_P = C_0 - (C_{P1}, C_{P2} \dots C_{Pn}) \begin{bmatrix} C_{11} & C_{12} & \dots & C_{1n} \\ C_{21} & C_{22} & \dots & C_{2n} \\ \cdot & \cdot & & \cdot \\ \cdot & \cdot & & \cdot \\ C_{n1} & C_{n2} & & C_{nn} \end{bmatrix}^{-1} \begin{bmatrix} C_{P1} \\ C_{P2} \\ \cdot \\ \cdot \\ C_{Pn} \end{bmatrix}. \quad (13)$$

The matrix  $[C_{ik}]$  of the autocovariances of geoid heights at the observed points is used to predict the geoid height and its error variance. The estimators (10) and (13) do not include the noise or measurement errors. However, the errors of the observed points can be included in the predictions by replacing  $C_{ik}$  in equations (9) and (12) with

$$\bar{C}_{ik} = C_{ik} + D_{ik}, \quad (14)$$

where

$$D_{ik} = M\{n_i n_k\}$$

is the autocovariance of the noise.

The error covariance is the correlation of the prediction errors  $\epsilon_P$  and  $\epsilon_Q$  at points P and Q,

$$\begin{aligned}
\sigma_{PQ} = M\{\epsilon_P \epsilon_Q\} = & C_{PQ} - \sum_{i=1}^n \sum_{k=1}^n C_{Pk} C_{ik}^{-1} C_{Qi} \\
& - \sum_{j=1}^{n'} \sum_{\ell=1}^{n'} C_{Q\ell} C_{j\ell}^{-1} C_{Pj} \\
& + \sum_{i=1}^n \sum_{k=1}^n \sum_{j=1}^{n'} \sum_{\ell=1}^{n'} C_{Pk} C_{ik}^{-1} C_{ij} C_{j\ell}^{-1} C_{Q\ell} \quad (15)
\end{aligned}$$

where the observed points  $(j, \ell)$  associated with point  $Q$  do not necessarily coincide with the  $(i, k)$  points. The relationship in equation (11) is a special case with  $P=Q$ .

#### B. Profile Prediction Method

Profile data may also be regarded as sample points of a continuous function. Then the methods of spectral analysis are available for the prediction of the gridded data base. The geoid height autocovariance function of Tscherning and Rapp [4] is used in the prediction of the mean geoid heights and the prediction error covariance function. The Fourier transform of the geoid height covariance function is the power spectrum of the geoid height field which is assumed to be isotropic. The transform changes the data on a flat surface from the time or space domain to the frequency domain. The Wiener theory of prediction is used to estimate the mean geoid heights and the prediction error spectrum in the frequency domain. Then the inverse Fourier transform of the error spectrum is the prediction error autocovariance. The profile prediction method is discussed in the appendix.



#### IV. ESTIMATION OF GRAVITY ANOMALIES

The gravity anomaly estimates presented in this report are computed from simulated geoid heights and are compared with gravity anomalies known to be consistent with the input geoid heights. This section introduces Stokes' integral and a method of localization. The localization is supported by a discussion of the contributions of distant zones and high degree harmonic coefficients to the computed geoid height. Effects of errors in the low degree harmonic coefficients of the earth gravitational model (EGM) are also considered.

##### A. Stokes' Integral

The geoid height  $N$  and the gravity anomaly  $\Delta g$  are related to the disturbing potential

$$T = W - U,$$

where  $W$  is the total gravity potential and  $U$  is the normal gravity potential (the potential field of the reference ellipsoid). The disturbing potential is representable as a harmonic series

$$T(\phi, \lambda) = \frac{GM}{R} \sum_{n=2}^{\infty} \sum_{m=0}^n [C_{nm} \cos m\lambda + S_{nm} \sin m\lambda] P_{nm}(\sin\phi). \quad (16)$$

$$(n, m) \neq (2, 0), (4, 0).$$

The gravity anomaly is defined in terms of the disturbing potential by

$$\Delta g = - \frac{\partial T}{\partial r} - \frac{2T}{r},$$

and the geoid height is defined by Bruns' equation

$$N = \frac{T}{\gamma}.$$



Stokes' integral makes it possible to compute  $N$  from  $\Delta g$  without working through the disturbing potential. Stokes' integral is

$$N(\phi, \lambda) = \frac{R}{4\pi\gamma} \int \int S(\psi) \Delta g(\phi', \lambda') \cos \phi' d\phi' d\lambda' \quad (17)$$

over an approximating sphere of mean radius  $R$  and mean gravity  $\gamma$ .

Stokes' function for the angular distance  $\psi$  between  $(\phi, \lambda)$  and  $(\phi', \lambda')$  is

$$S(\psi) = \frac{1}{\sin(\frac{\psi}{2})} - 6 \sin(\frac{\psi}{2}) + 1 - 5 \cos \psi - 3 \cos \psi \ln[\sin(\frac{\psi}{2}) + \sin^2(\frac{\psi}{2})] \quad (18)$$

for points on the unit sphere [5].

Stokes' integral is ordinarily used to compute geoid heights by worldwide integration of the gravity anomaly field. For this purpose the integral is replaced by the discrete form

$$N(\phi, \lambda) = \frac{R}{4\pi\gamma} \sum_{\phi'} \sum_{\lambda'} S(\psi) \overline{\Delta g}(\phi', \lambda') \cos \phi' \Delta \phi' \Delta \lambda' \quad (19)$$

with some provision for dealing with the singularity of  $S(\psi)$  at  $\psi=0$ , and  $\overline{\Delta g}$  is the mean gravity anomaly over an element with center  $(\phi', \lambda')$ .

Stokes' integral may also be regarded as an integral equation for the inverse problem of estimating anomalies from geoid heights. Then the discrete form (19) becomes a worldwide linear algebraic system

$$Ax = b,$$

where  $A$  is the coefficient matrix of values of Stokes' function,  $b$  is the data vector of geoid height values, and  $x$  is the system

parameter vector of gravity anomalies. Since reliable geoid height values are not available for much of the world and the worldwide algebraic system is much too large to estimate the vector  $x$  over a one degree grid, a method of localization of the computations is needed. That is, there is a need to restrict the data and computations for Stokes' integral equation to a relatively small local region. The next section proposes a method of localization which consists of estimating the global (long wave length) harmonics with the earth gravitational model of a world geodetic system, and then estimating the high degree (short wave length) components over a small local region.

#### B. Localization of Stokes' Integral Equation

Each of the functions  $N$ ,  $S(\psi)$ , and  $\Delta g$  involved in Stokes' integral equation is harmonic and expandable in a series of Legendre associated functions. The harmonic series are

$$N(\phi, \lambda) = \frac{GM}{R_Y} \sum_{n=2}^{\infty} \sum_{m=0}^n [(C_{nm} \cos m\lambda + S_{nm} \sin m\lambda) P_{nm}(\sin\phi)], \quad (20)$$

$$S(\psi) = \sum_{n=2}^{\infty} \frac{2n+1}{n-1} P_n(\cos\psi), \quad (21)$$

$$\begin{aligned} P_n(\cos\psi) &= P_n(\cos\phi) P_n(\cos\phi') \\ &+ 2 \sum_{m=1}^n \frac{(n-m)!}{(n+m)!} [\cos m\lambda P_{nm}(\sin\phi) \cos m\lambda' P_{nm}(\sin\phi') \\ &+ \sin m\lambda P_{nm}(\sin\phi) \sin m\lambda' P_{nm}(\sin\phi')], \quad (22) \end{aligned}$$

$$\Delta g(\phi, \lambda) = \frac{GM}{R^2} \sum_{n=2}^{\infty} \sum_{m=0}^n (n-1) [C_{nm} \cos m\lambda + S_{nm} \sin m\lambda] P_{nm}(\sin \phi), \quad (23)$$

where  $(n,m) \neq (2,0), (4,0)$ .

Since the Legendre functions are orthogonal, they are linearly independent so that  $N$ ,  $S(\psi)$ , and  $\Delta g$  may be decomposed into high and low degree components. Figure 5 shows the effect of removing lower harmonics from Stokes' function, with the full function and three residual forms being shown. The high degree (short wave length) components have short distance effects and the low degree components have long range effects.

Linearity of the integral allows a corresponding decomposition of the surface of the earth according to distance from the point of estimation. Then the worldwide integral is the sum of the integrals over a near region  $R_1$  and a distant region  $R_2$  such that the two regions together cover the surface of the earth. In this report it is assumed that the low degree component of Stokes' function consists of harmonic degrees 2-12 and the high degree component consists of degrees 13- $\infty$ . It is further assumed that the region  $R_1$  has a radius not less than  $5^\circ$  for  $1^\circ \times 1^\circ$  estimation.

By means of the decompositions mentioned above, Stokes' integral equation may be written

$$N(\phi, \lambda) = K \int_{R_1} \int S_{2-12}(\psi) \Delta g_{2-12}(\phi', \lambda') \cos \phi' d\phi' d\lambda'$$

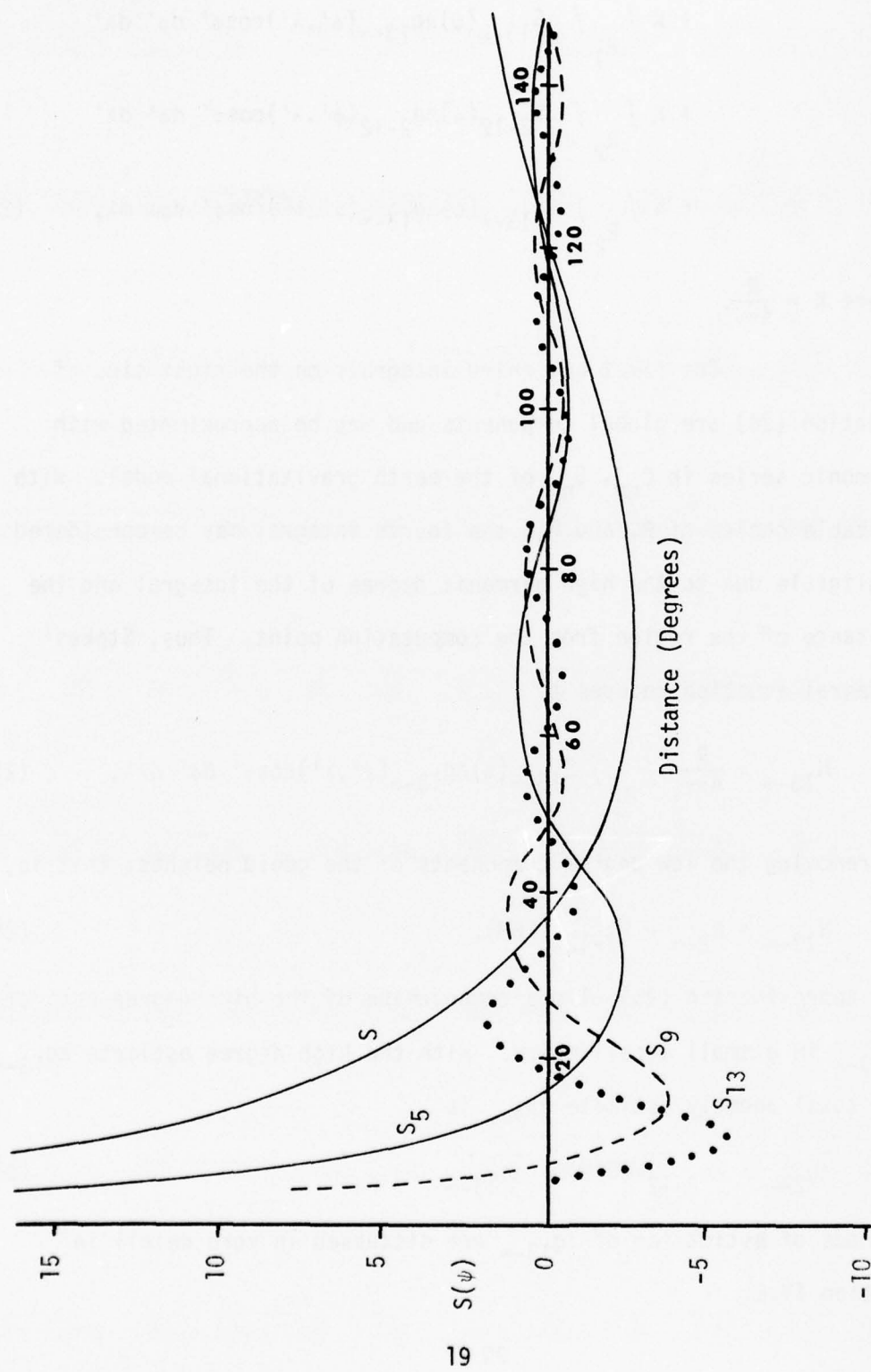


Figure 5. Stokes' Kernel Function with Low Degree Harmonics Removed.



$$\begin{aligned}
& + K \int_{R_1} \int S_{13-\infty}(\psi) \Delta g_{13-\infty}(\phi', \lambda') \cos \phi' d\phi' d\lambda' \\
& + K \int_{R_2} \int S_{2-12}(\psi) \Delta g_{2-12}(\phi', \lambda') \cos \phi' d\phi' d\lambda' \\
& + K \int_{R_2} \int S_{13-\infty}(\psi) \Delta g_{13-\infty}(\phi', \lambda') \cos \phi' d\phi' d\lambda', \quad (24)
\end{aligned}$$

where  $K = \frac{R}{4\pi\gamma}$ .

The first and third integrals on the right side of equation (24) are global components and may be approximated with harmonic series in  $C_{nm}$ ,  $S_{nm}$  of the earth gravitational model. With suitable choice of  $R_1$  and  $R_2$ , the fourth integral may be considered negligible due to the high harmonic degree of the integral and the distance of the region from the computation point. Thus, Stokes' integral equation reduces to

$$N_{13-\infty} \approx \frac{R}{4\pi\gamma} \int_{R_1} \int S_{13-\infty}(\psi) \Delta g_{13-\infty}(\phi', \lambda') \cos \phi' d\phi' d\lambda', \quad (25)$$

by removing the low degree components of the geoid heights; that is,

$$N_{13-\infty} = N_{2-\infty} - N_{2-12} \text{ (EGM)}. \quad (26)$$

The approximation (25) allows computation of the high degree estimate  $\tilde{\Delta g}_{13-\infty}$  in a small local region. With the high degree estimate  $\tilde{\Delta g}_{13-\infty}$ , the total anomaly estimate  $\tilde{\Delta g}_{2-\infty}$  is

$$\tilde{\Delta g}_{2-\infty} = \Delta g_{2-12} \text{ (EGM)} + \tilde{\Delta g}_{13-\infty}. \quad (27)$$

Methods of estimation of  $\tilde{\Delta g}_{13-\infty}$  are discussed in more detail in Section IV.E.

C. Contributions of Distant Zones and High Harmonic Degrees  
To Computed Geoid Height

The expected error variance  $\sigma^2(N)$  of the computed geoid height due to neglect of gravity anomaly data beyond a region of radius  $\psi_0$  and harmonic degree greater than K is, from Heiskanen and Moritz [5],

$$\sigma^2(N) = \frac{R^2}{4\gamma^2} \sum_{n=K+1}^{\infty} Q_n^2 C_n \quad (28)$$

where

$$Q_n = \int_{\psi_0}^{\pi} S(\psi) P_n(\cos\psi) \sin\psi \, d\psi, \quad (29)$$

$C_n$  is the degree variance of degree n,

$S(\psi)$  is Stokes' function of angular distance  $\psi$ .

Computed results for the degree variances of the test model are shown graphically in Figure 6. The graph shows the expected error in geoid heights due to neglecting gravity anomaly data outside a circle of radius  $\psi_0$  and harmonics above  $n = 8, 12$ , and  $18$ . For high degree components above degree 12, the graph shows that the expected error for  $\psi_0 = 5^\circ$  is approximately 1.5 meters.

The inverse problem of estimating the expected error variance  $\sigma^2(\Delta g)$  of gravity anomalies due to neglect of high degree harmonics and distant regions is much more difficult. The error variance for geoid heights suggests that high degree gravity anomaly components of degree greater than 12 may be effectively estimated

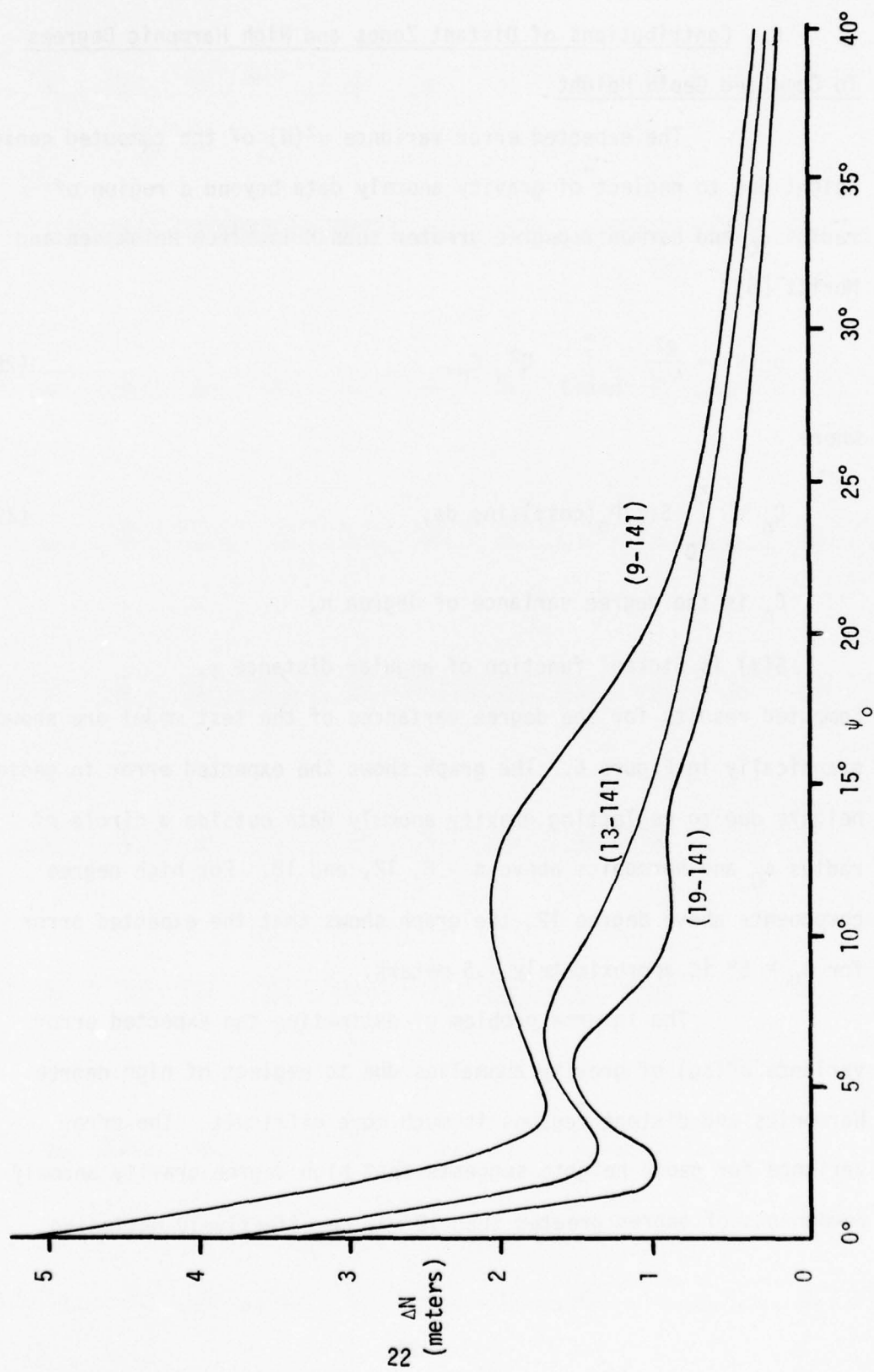


Figure 6. Expected Error in  $N$  Due to Exclusions of Distant Zones.

by neglecting geoid height data at distances greater than  $5^\circ$ . It is assumed that the fourth integral, over  $R_2$ , of equation (24) is negligible since the high degree Stokes' function is effectively damped out for the distances included in this integral (Figure 5). The present series of tests is a more specific justification for this assumption than the statistical method discussed above.

#### D. Effects of Errors in the Low Degree Component

Errors in the low degree harmonic coefficients are not related to the satellite altimetry data, but are included in the computational process by means of the supplementary data. They have a two-fold effect on the estimated gravity anomalies, which can be seen by analyzing the computational process. They affect the high degree gravity anomaly estimates by being included in the geoid height data used in the recovery process, and also they have an effect on the low degree component since it is computed from the coefficients. An estimate of the magnitude of this effect was determined by repeating the recovery process with perturbed coefficients. The results of this analysis show that the effect on the geoid height values is  $\pm 0.6$  meters, which causes an error of  $\pm 0.2$  mgal in the high degree component of the gravity anomalies. The effect of these errors on the low degree components is about  $\pm 0.7$  mgal, and therefore the combined effect on the gravity anomalies is  $\pm 0.7$  mgal. These errors in the harmonic coefficients will be reduced by updating the earth gravitational model as geoid height data from satellite altimetry becomes available.



### E. Method of Estimating Anomalies

The discrete form of  $N_{13-\infty}(R_1)$ , equation (25), may be solved as a linear algebraic system

$$Ax = b, \quad (30)$$

where  $A$  is the coefficient matrix with one row and one column for each square in region  $R_1$ . For a least squares estimator,  $R_1$  may be decomposed into an inner and outer region with

$$Ax + v = b, \quad (31)$$

where  $v$  is the residual vector and  $A$  has one row for each square in the outer region and one column for each square in the inner region.

With the least squares estimator, anomalies are estimated only in the inner region and there is a loss of information in the outer region. Both methods of estimation lose accuracy near the boundary. These errors of localization affect the parameter vector  $x$  and the coefficient matrix  $A$  so that the errors carry over to all elements of the covariance matrix. Thus, even though only the estimate of the central square is accepted for each run, the corresponding element of the covariance matrix is dominated by localization error and the estimation error must be evaluated by some other method.

Most of the test runs presented in this report were made with an unweighted least squares estimator. Then the estimator  $\hat{x}$  of  $x$  for equation (31) is

$$\hat{x} = (A^T A)^{-1} A^T b. \quad (32)$$

The outer region was  $11^\circ \times 11^\circ$  and the inner region was  $5^\circ \times 5^\circ$ . The singularity of  $S(\psi)$  was avoided by arbitrarily offsetting by eight

minutes from  $\psi = 0$ . The program was modified for iterative improvement of two estimated anomaly fields. Estimation errors were computed by subtracting anomalies known to be consistent with the input geoid heights from the estimated anomalies.

In these computations, the eight minute offset of  $S(0)$  was used to avoid the singularity of Stokes' function. However, additional tests suggest that a larger offset may have been better for the  $1^\circ \times 1^\circ$  estimates. An optimum offset of 18' was selected after analyzing offset values out to about 21' from the computation point. Moritz [5] discusses a method in which the size of the offset depends on both the size of the square and the probable error of the geoid field. Further study of this approach is being carried on at this Center.

It is also possible to introduce a local correction to the harmonic coefficient  $C_{00}$  or the equatorial radius  $a$ . This might be done by subtracting the mean geoid height over the integration region from the geoid height of each one degree square or by inserting a column of ones into the design matrix  $A$  of the least squares estimator to estimate the local bias. The use of weight matrices has not been completely tested. The best weight matrix for this purpose appears to be the inverse of the geoid height covariance matrix. A least squares estimator weighted in this way becomes a minimum variance estimator. Another procedure that will be investigated is the use of initial estimates of the gravity anomalies based on existing gravity

observations. The computer program could be modified for any of these methods. A computer program for least squares collocation [6] is being prepared to continue these lines of investigation.

## V. TEST DATA SIMULATION

Tests were conducted to demonstrate that gravity anomalies can be predicted from local geoid heights with sufficient accuracy to make effective use of GEOS-III altimetric geoid height data. Testing of the computational method described earlier requires consistent sets of simulated high frequency geoid heights and gravity anomalies. In some of the tests, the geoid heights were modified by the introduction of random errors or by smoothing to simulate mean values.

Three methods of developing consistent sets of high frequency geoid heights and gravity anomalies are considered feasible: the gravity anomaly method, the point mass method, and the harmonic method. In the first method, a gravity anomaly field is assumed and the geoid heights are computed with Stokes' integral and worldwide integration. In the second method, a point mass set replaces the mass of the earth in the computations and both the gravity anomaly field and the geoid height field are computed from the disturbing potential field of the point mass set. In the third method, a set of harmonic coefficients to high degree and order is constructed and both the gravity anomaly and geoid height fields are computed by harmonic series. The last method appears to be the simplest and most consistent since no worldwide integration is involved. Moreover, the exact harmonic structure of the data is known so that separation of the high and low degree components of geoid heights or gravity anomalies is simple.



In order to produce a gridded data base whose exact harmonic content is known for testing the estimation of gravity anomalies, it was decided to generate the data base from a hypothetical harmonic model consisting of spherical harmonic coefficients to degree and order 18 from an existing earth gravitational model and fictitious coefficients beginning from degree 19 through degree and order 141. The fictitious coefficients were generated by Kaula's approximate formula [7]

$$C_n = \frac{192}{n(1+\frac{3}{2n})} \text{ mgal}^2 \quad (33)$$

and the harmonic form

$$C_n = M\{\Delta g_n^2\} = \sum_{m=0}^n (\bar{A}_{nm}^2 + \bar{B}_{nm}^2) \quad (34)$$

so that all  $\bar{A}$  and  $\bar{B}$  of degree  $n$  have the same magnitude and random signs, and the  $C_n$  in equations (33) and (34) agree. The  $\bar{A}_{nm}$ ,  $\bar{B}_{nm}$  were transformed to  $C_{nm}$ ,  $S_{nm}$  which were used to compute compatible sets of geoid heights and gravity anomalies at center points of  $1^\circ \times 1^\circ$  elements of a  $50^\circ \times 50^\circ$  block with

$$N(\phi, \lambda) = \frac{GM}{R_Y} \sum_{n=2}^{141} \sum_{m=0}^n (C_{nm} \cos m\lambda + S_{nm} \sin m\lambda) P_{nm}(\sin\phi), \quad (35)$$

$$\Delta g(\phi, \lambda) = \frac{GM}{R^2} \sum_{n=2}^{141} (n-1) \sum_{m=0}^n (C_{nm} \cos m\lambda + S_{nm} \sin m\lambda) P_{nm}(\sin\phi). \quad (36)$$

A  $10^\circ \times 10^\circ$  block located in the center of the data was selected for testing and the geoid heights were input to the estimation program which subtracted the low degree component and then estimated high degree anomalies from the high degree geoid heights. The low degree component  $\Delta g(2-12)$  of the anomaly field was added to the estimated  $\tilde{\Delta g}(13-141)$  and the results compared with the simulated  $\Delta g(2-141)$ . Although the simulated gravity anomalies are not intended to represent the physical values, they are consistent with the simulated geoid heights. Hence, the differences between the estimated gravity anomalies and the simulated values are the errors of estimation. Figure 7 is a flow chart of the test procedure for the hypothetical model.

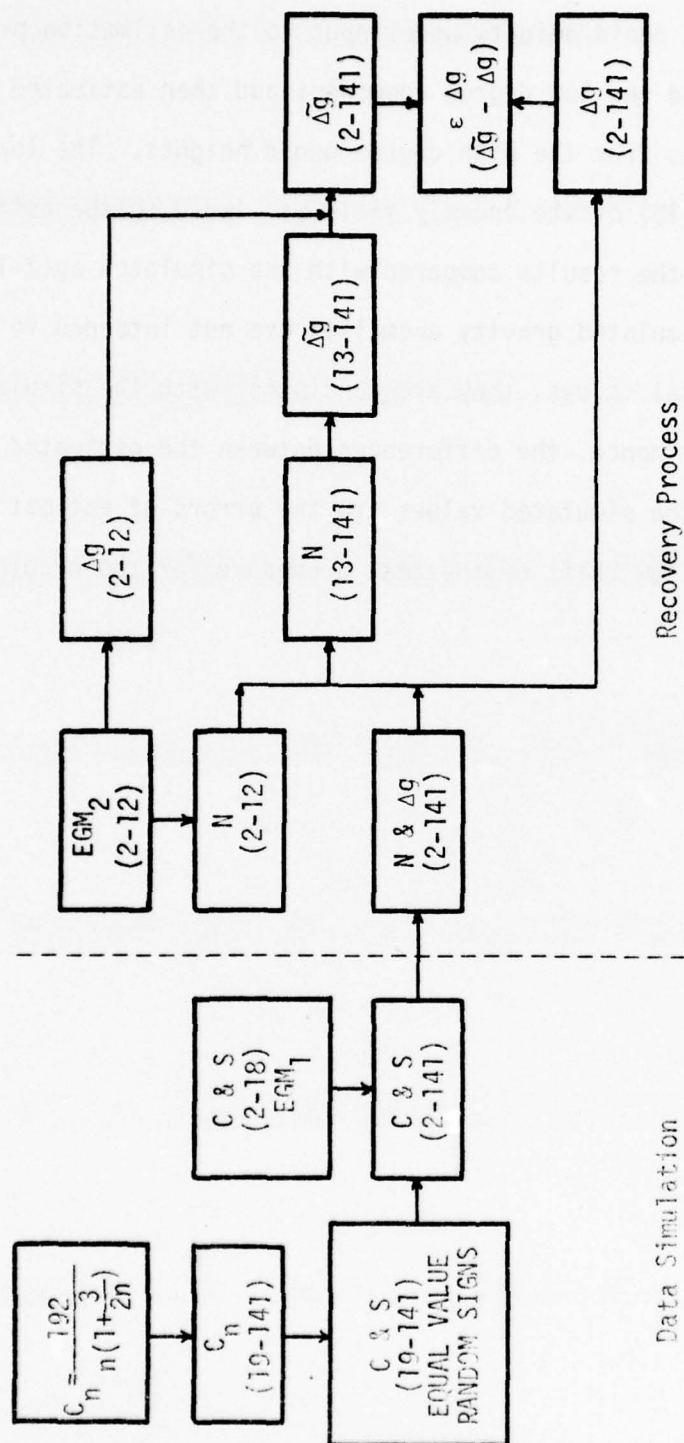


Figure 7. GEOS-III Spherical Harmonic Model Test.

## VI. PROGRAM INPUT AND TEST RESULTS

Results from the estimation of gravity anomalies of one hundred  $1^\circ \times 1^\circ$  squares in a  $10^\circ \times 10^\circ$  block from simulated input data and the associated estimation errors are displayed in tabular and graphic form. The graphics include contour plots of the data and amplitude spectra. Mean gravity anomaly values were simulated in these computations by a smoothing operation. The effect of measurement error in the geoid height values was approximated by adding random noise to the data.

Contour plots of the geoid heights and gravity anomalies at the centers of  $1^\circ \times 1^\circ$  squares for the full spherical harmonic set ( $n,m = 2-141$ ) are shown in Figures 8 and 9, respectively. These fields are considered errorless. Point gravity anomalies from the high degree component ( $n,m = 13-141$ ) of the anomaly field for each  $1^\circ \times 1^\circ$  element are shown in Table 1. A set of  $1^\circ \times 1^\circ$  mean gravity anomalies was simulated by applying two-dimensional smoothing to the high degree anomaly field. The smoothed value for each element is one-half its raw value plus one-eighth of the sum of the values of the four adjacent squares. The smoothed field is shown in Table 2.

The gravity anomalies estimated from gridded geoid heights for  $1^\circ \times 1^\circ$  elements are shown in Table 3. To determine the estimation errors for each  $1^\circ \times 1^\circ$  element, differences were computed between the gravity anomaly estimates (Table 3) and both the reference point values of Table 1 and the reference mean values of Table 2.



39°N

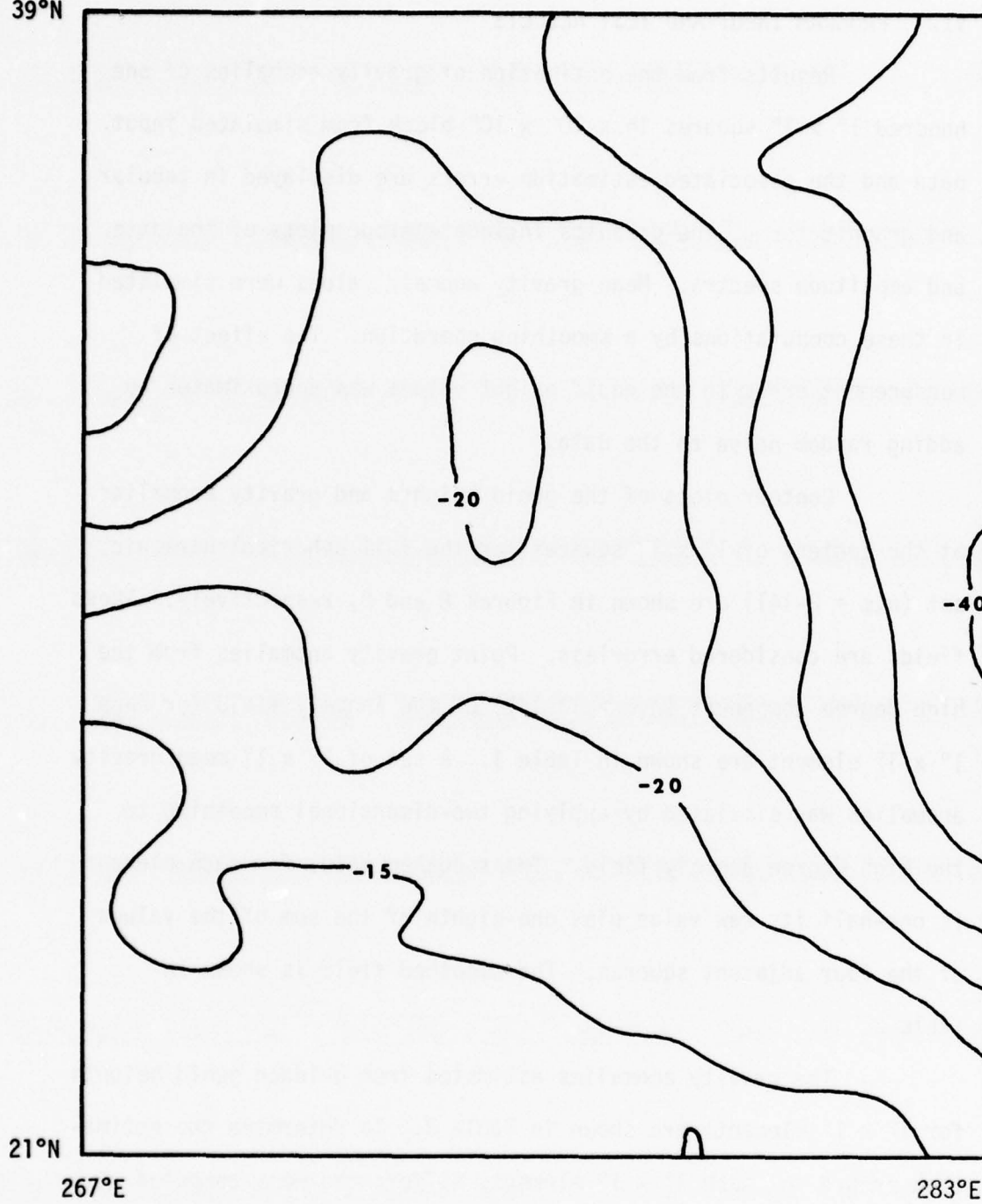


Figure 8. Hypothetical Geoid Heights ( $n,m=2-141$ ) (meters).

39°N

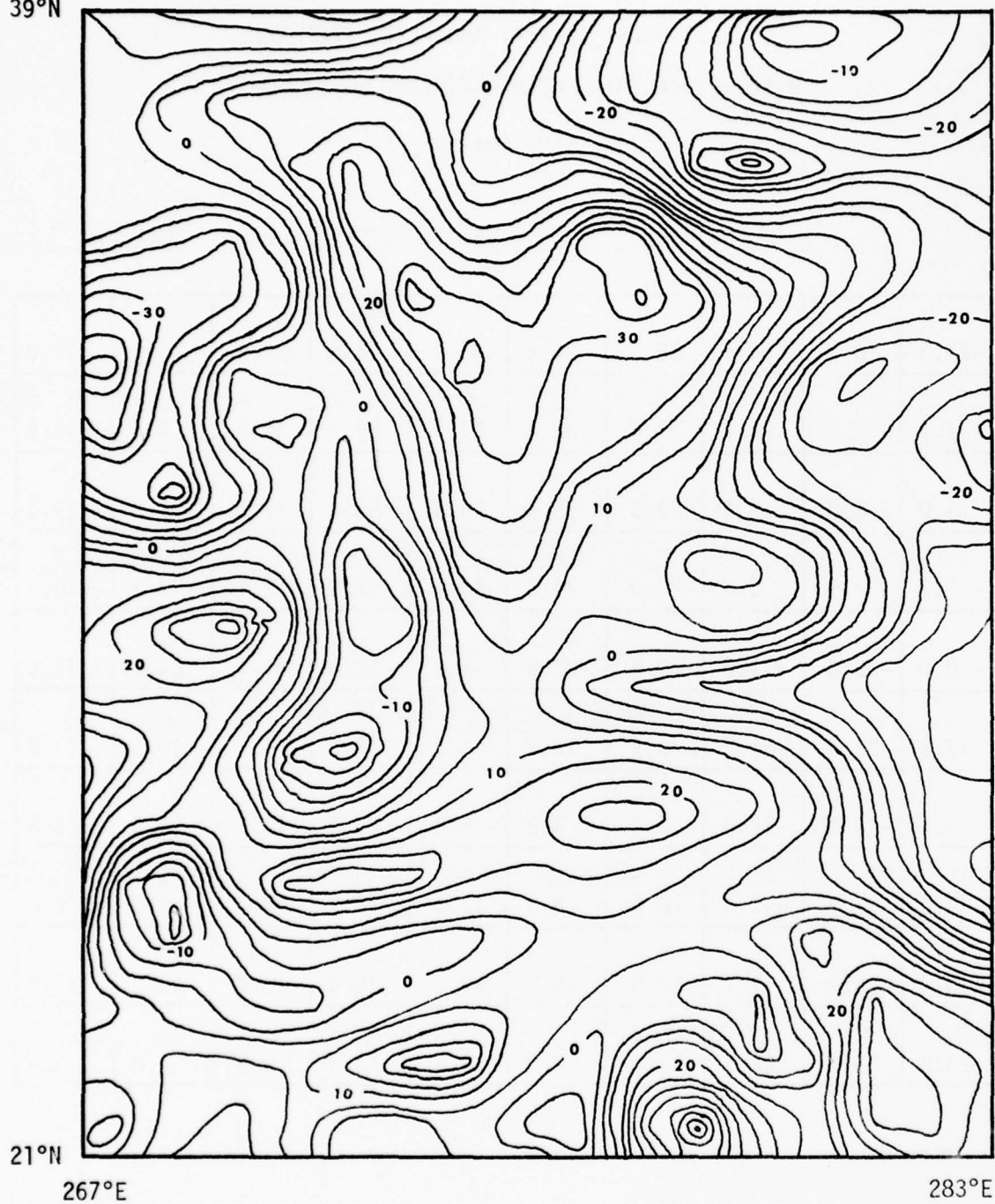


Figure 9. Hypothetical Gravity Anomalies ( $n, m=2+141$ ) (mgal).

Table 1  
1° x 1° POINT GRAVITY ANOMALIES FROM THE  
HYPOTHETICAL HIGH DEGREE FIELD n,m = 13-141  
( $\Delta g$ , mgal)

-21.5	12.7	38.1	33.7	26.6	36.6	46.4	39.9	25.4	13.6
- 7.1	- 3.2	20.7	37.8	32.1	24.5	29.4	26.7	4.6	-15.9
4.0	- 8.0	3.6	29.5	33.6	25.4	25.6	17.7	- 6.3	-21.1
- 3.1	- 8.3	3.5	28.0	27.5	13.4	11.0	7.7	- 3.3	-10.9
- 0.8	-22.3	-11.6	20.0	22.9	9.6	12.1	21.4	24.1	15.6
13.9	-22.4	-22.2	6.7	13.7	4.3	6.8	15.6	18.5	11.8
3.4	-14.6	-12.3	3.4	4.2	- 6.0	-11.2	-12.3	-14.0	-18.5
-27.0	-32.7	-16.0	0.6	8.0	12.0	12.1	10.2	9.6	2.0
-10.4	-14.0	1.7	10.5	15.5	25.7	28.4	22.7	19.5	12.6
23.5	23.9	22.1	13.2	9.0	13.7	13.3	6.9	4.8	3.9

MEAN VALUE = 8.7 mgal

RMS = 19.0 mgal

Table 2

1° x 1° SMOOTHED MEAN GRAVITY ANOMALIES FROM  
THE HYPOTHETICAL HIGH DEGREE FIELD  $n,m = 13 \rightarrow 141$

( $\overline{\Delta g}$ , mga1)

-15.3	11.0	31.1	31.1	28.1	30.8	41.6	34.0	19.9	9.1
- 6.6	0.7	19.9	33.4	31.4	27.7	30.1	24.8	6.0	-10.8
- 0.3	- 4.5	7.5	27.6	31.1	24.8	23.2	15.6	- 3.4	-12.7
- 4.5	- 7.9	3.2	24.1	26.0	15.9	12.8	9.7	0.2	- 8.3
- 1.1	-16.5	- 8.4	15.8	20.3	11.4	12.2	18.1	18.6	10.3
8.6	-16.8	-16.0	5.2	11.6	5.2	6.0	12.1	13.9	7.5
- 3.4	-11.5	-12.3	1.6	4.5	- 1.8	- 5.5	- 6.1	- 7.3	-12.2
-18.8	-25.3	-13.3	1.0	8.0	11.0	11.0	9.1	7.0	- 0.4
- 6.5	- 9.2	1.2	9.1	14.4	21.6	23.4	19.5	16.0	8.7
14.3	12.0	14.9	10.6	9.6	13.4	13.3	9.1	7.9	6.4

MEAN VALUE = 8.3 mga1

RMS = 16.3 mga1



Table 3

1° x 1° ESTIMATED GRAVITY ANOMALIES FROM GRIDDED GEOID

USING THE HYPOTHETICAL HIGH DEGREE FIELD  $n, m = 13 \rightarrow 141$

( $\Delta\tilde{g}$ , mga1)

-14.2	9.8	27.9	28.0	25.5	31.6	36.0	29.5	17.7	8.1
- 5.9	0.8	17.8	29.8	28.2	24.4	25.7	21.2	5.3	9.1
0	- 2.4	7.6	24.1	27.4	22.7	20.9	13.9	- 2.1	-13.3
- 3.3	- 3.8	5.7	21.7	23.3	15.5	12.8	9.1	0.5	- 7.0
- 0.8	-10.8	- 3.5	15.0	18.3	11.7	12.0	15.5	14.8	7.4
7.3	-10.5	- 9.3	6.6	11.5	6.9	7.3	10.8	10.7	4.7
1.8	- 7.9	- 5.7	3.9	6.0	1.4	- 1.5	- 2.7	- 5.0	- 9.6
-12.3	-16.1	- 6.9	3.5	8.8	11.3	11.1	9.1	6.8	0.5
- 2.9	- 4.6	3.3	9.0	12.8	18.2	19.6	16.4	13.4	7.8
13.3	14.0	13.6	10.5	9.8	13.3	13.7	10.6	9.3	7.6

5° x 5° INTEGRATION

MEAN VALUE = 8.5 mga1

RMS = 11.5 mga1

For this evaluation, Tables 1 and 2 are considered errorless. The differences are shown in Tables 4 and 5, respectively. The root mean square (RMS) error of estimates from point data is 6.1 mgal and the RMS error of estimates from mean data is 2.9 mgal. Thus,  $1^\circ \times 1^\circ$  estimates are better in comparison with mean data than with point data.

Input and output data fields were analyzed by spectral methods for their harmonic frequency content. Contour plots of the amplitude spectra are shown in Figures 10 to 14. The sampling interval on the contour plots is a one degree increment of latitude or longitude between data points. The coordinate axes are frequencies of the Fourier representation of gravity anomalies or estimation errors. The wave lengths in degrees are reciprocals of the frequencies. The axes are in the direction of increasing frequency and decreasing wave length.

The amplitude spectra of gravity anomalies and errors were computed as though the data points were on a plane. Contours of amplitude spectra for isotropic fields over a plane are arcs of concentric circles. Curvature of the surface and convergence of meridians distort the contours of an isotropic field to elliptical arcs. If the field is not isotropic, then the contours are distorted accordingly.

The contour plots of amplitude spectra in Figures 10, 11 and 12 show that the fields are approximately isotropic in the long wave lengths. There is distortion in the contours of the high

Table 4  
 ERROR OF ESTIMATION ( $\Delta\tilde{g} - \Delta g$ )  
 FOR 1° x 1° POINT VALUES  
 (mgal)

7.3	- 2.9	-10.2	- 5.7	- 1.1	- 5.0	-10.4	-10.4	- 7.7	- 5.5
1.2	4.0	- 2.9	- 8.0	- 3.9	- 0.1	- 3.7	- 5.5	0.7	6.8
- 4.0	5.6	4.0	- 5.4	- 6.2	- 2.7	- 4.7	- 3.8	4.2	7.8
- 0.2	4.5	2.2	- 6.3	- 4.2	2.1	1.8	1.4	3.8	3.9
- 0.0	11.5	8.1	- 5.0	- 4.6	2.1	- 0.1	- 5.9	- 9.3	- 8.2
- 6.6	11.9	12.9	- 0.1	- 2.2	2.6	0.5	- 4.8	- 7.8	- 7.1
- 1.6	6.7	6.6	0.5	1.8	7.4	9.7	9.6	9.0	8.9
14.7	16.6	9.1	2.9	0.8	- 0.7	- 1.0	- 1.1	- 2.8	- 1.5
7.5	9.4	1.6	- 1.5	- 2.7	- 7.5	- 8.8	- 6.3	- 6.1	- 4.8
-10.2	- 9.9	- 8.5	- 2.7	0.8	- 0.4	0.4	3.7	4.5	3.7

5° x 5° INTEGRATION

MEAN VALUE = -0.2 mgal

RMS = 6.1 mgal

Table 5  
 ERROR OF ESTIMATION ( $\Delta\bar{g} - \overline{\Delta g}$ )  
 FOR 1° x 1° MEAN VALUES  
 (mgal)

1.1	-1.2	- 3.2	- 3.1	- 2.7	0.8	- 5.5	- 4.5	- 2.2	- 1.0
0.7	0.2	- 2.1	- 3.6	- 3.3	- 3.4	- 4.3	- 3.6	- 0.7	1.6
0.3	2.1	0.1	- 3.5	- 3.7	- 2.2	- 2.3	- 1.7	1.3	- 0.5
1.2	4.1	2.4	- 2.4	- 2.8	- 0.3	0	- 0.6	0.3	1.4
0.3	5.7	4.8	- 0.9	2.0	0.3	- 0.2	- 2.6	- 3.8	- 2.9
-1.4	6.4	6.8	1.4	0.1	1.7	1.3	- 1.3	- 3.3	- 2.9
5.2	3.6	6.6	2.3	1.4	3.3	4.1	3.4	2.3	2.6
6.5	9.2	6.4	2.5	0.8	0.3	0	0	- 0.1	0.9
3.6	4.6	2.1	- 0.1	- 1.6	- 3.4	- 3.8	- 3.1	- 2.6	- 0.9
-1.0	2.0	- 1.3	- 0.2	0.2	- 0.1	0.4	1.5	1.4	1.3

5° x 5° INTEGRATION

MEAN VALUE = 0.2 mgal

RMS = 2.9 mgal



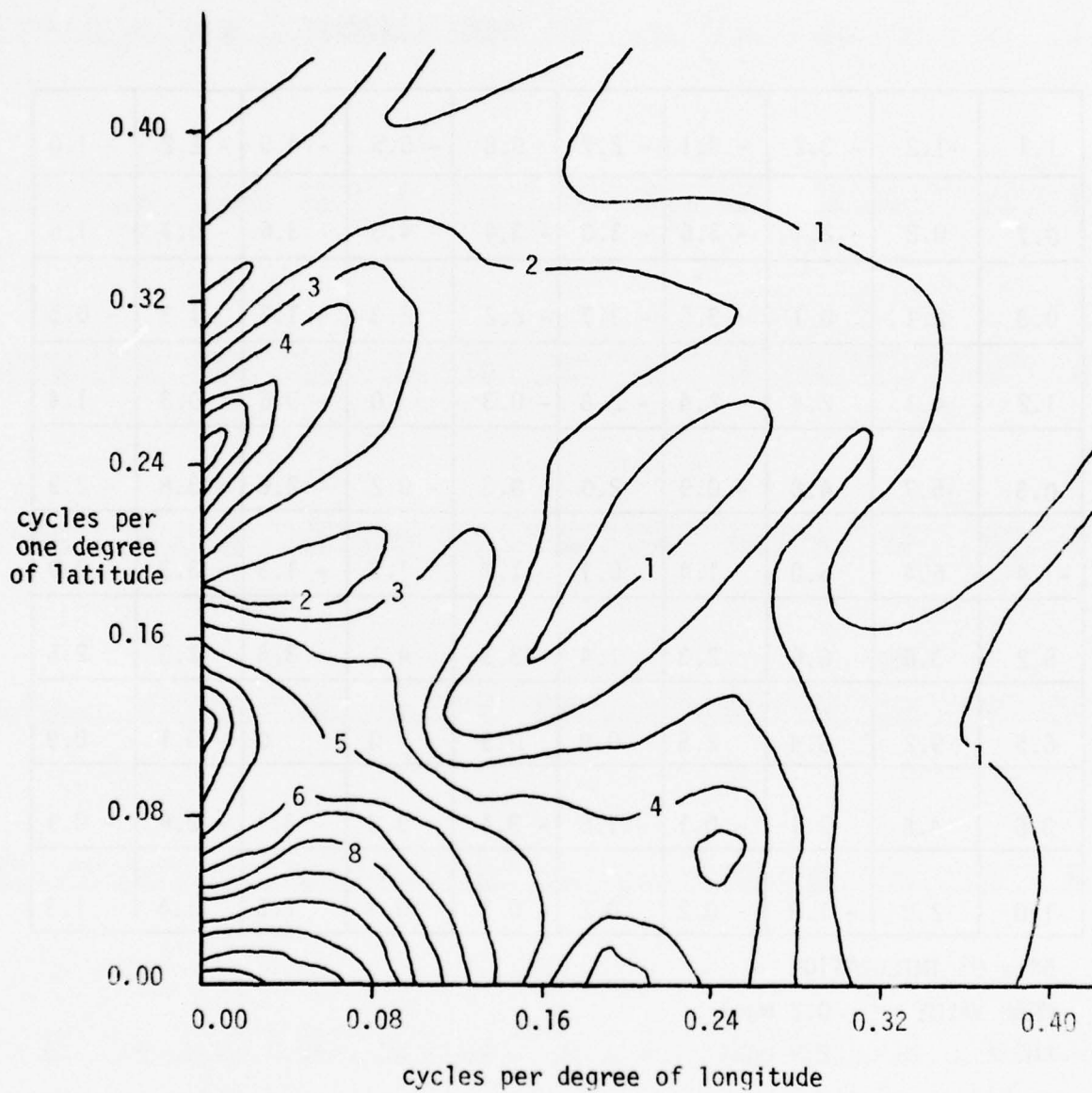


Figure 10. Amplitude Spectrum of  $1^\circ \times 1^\circ$  Point Gravity Anomalies ( $\Delta g$ ).

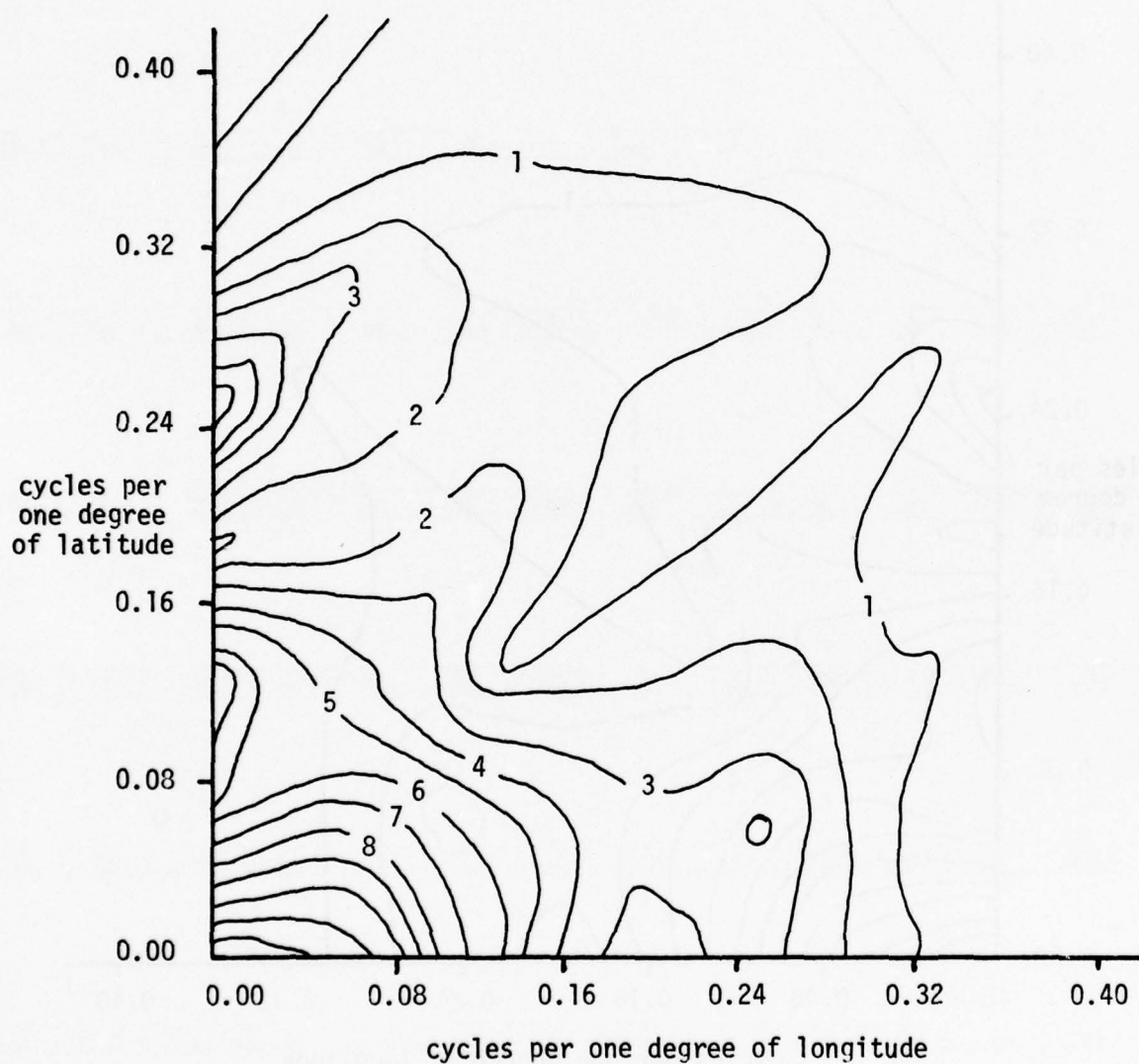


Figure 11. Amplitude Spectrum of  $1^\circ \times 1^\circ$  Mean Gravity Anomalies ( $\overline{\Delta g}$ ).

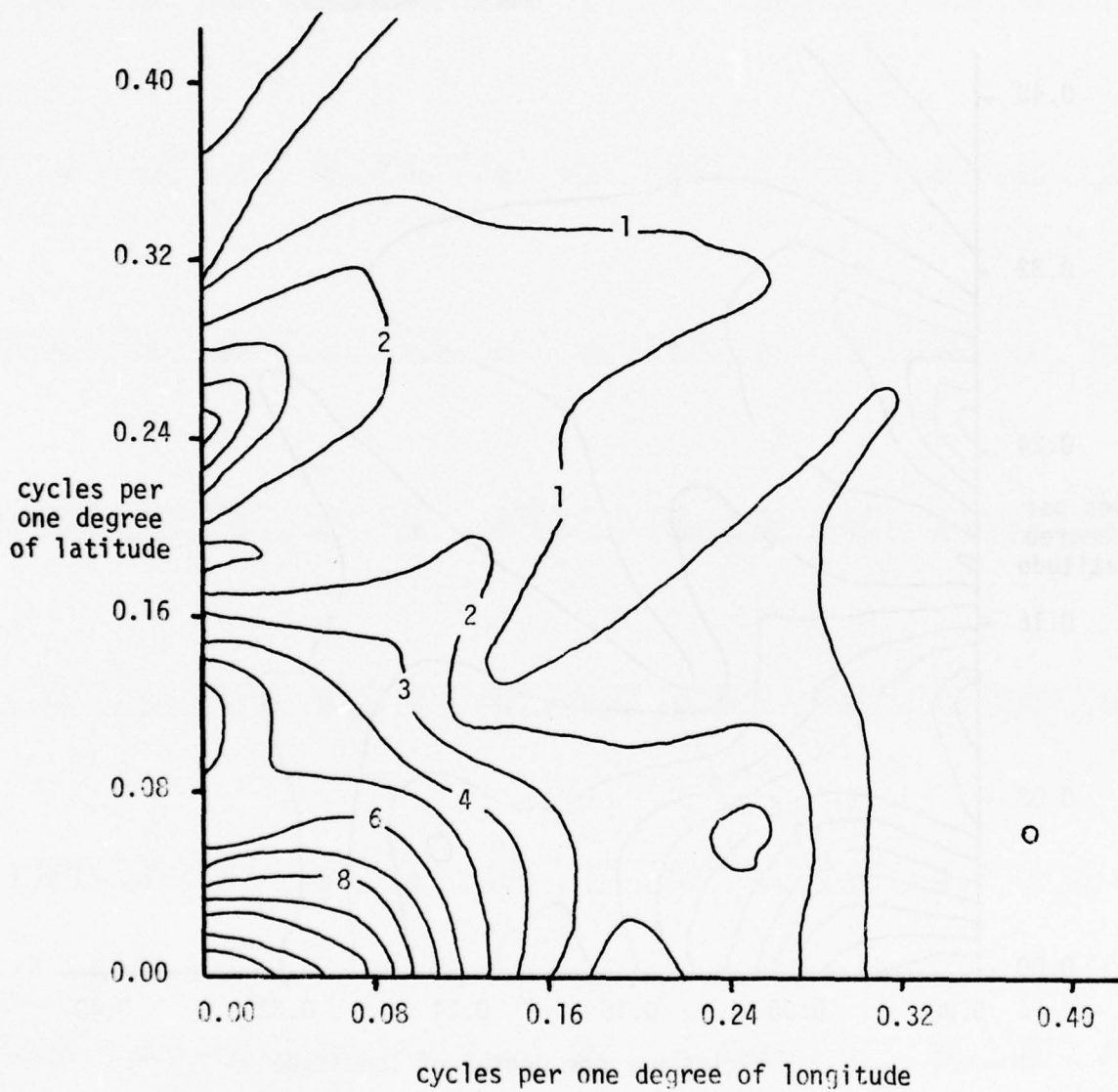


Figure 12. Amplitude Spectrum of 1° x 1° Estimated Gravity Anomalies ( $\Delta g$ ).

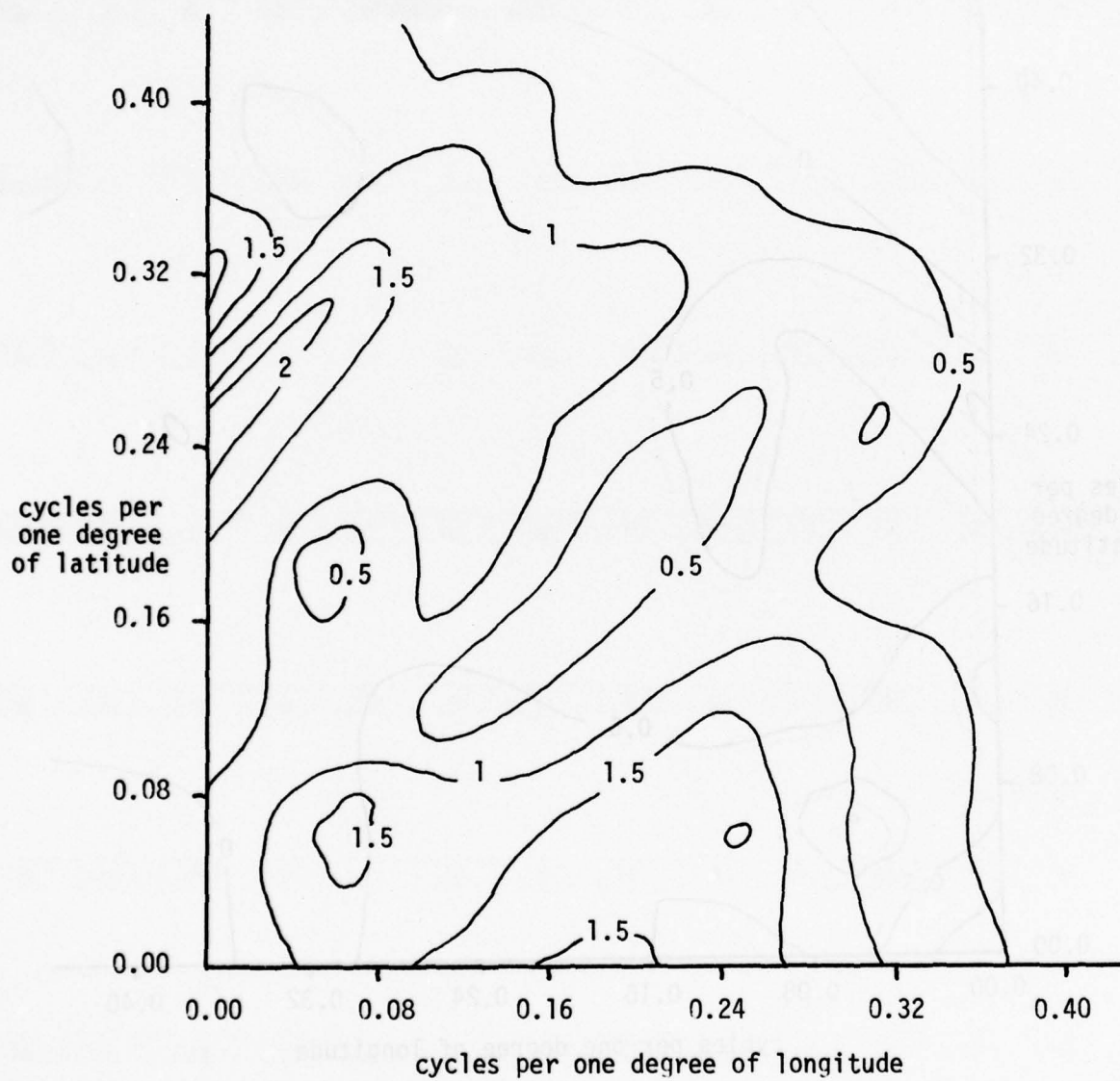


Figure 13. Amplitude Spectrum of  $1^\circ \times 1^\circ$  Estimation Errors ( $\Delta\tilde{g}-\Delta g$ ).



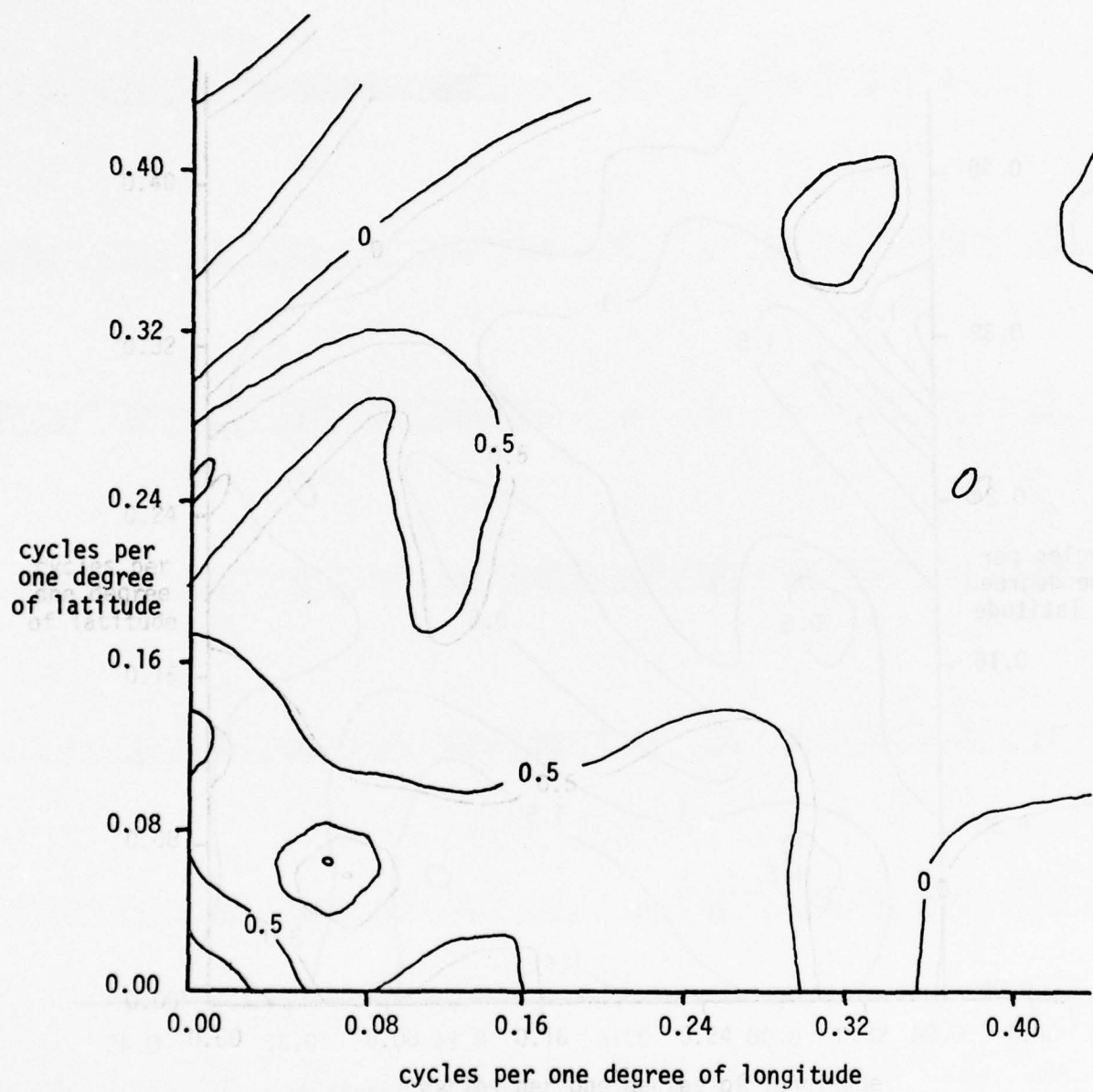


Figure 14. Amplitude Spectrum of  $1^\circ \times 1^\circ$  Estimation Errors ( $\overline{\Delta g - \Delta g}$ ).

frequency components. Comparison of spectra for point gravity anomalies ( $\Delta g$ ) and mean (smoothed) gravity anomalies ( $\overline{\Delta g}$ ) shows that there is a loss of high frequency in smoothing. Figures 11 and 12 are almost identical. This indicates that the estimated gravity anomaly field and the smoothed gravity anomaly field have very nearly the same Fourier harmonic content. The closer similarity of amplitude spectra for smoothed values and estimated values is corroborated by the spectra for estimation errors in Figures 13 (estimated minus point values) and 14 (estimated minus mean).

The preceding results were obtained with an errorless geoid height field. Since measurement necessarily involves error, the effects of random error and bias in the geoid field were investigated and the results shown in Tables 6 and 7. A random error field with a distribution of zero mean ( $\mu=0$ ) and standard deviation ( $\sigma$ ) of one meter was added to the geoid field. The error of estimation for each  $1^\circ$  is the difference between the resulting predicted anomalies ( $\hat{\Delta g}$ ) and the simulated mean anomalies (Table 6). Inclusion of the  $\mu=0$ ,  $\sigma=1m$  errors in the geoid field increases the RMS anomaly error from 2.9 mgal to 9.0 mgal with no significant change in the mean error. A one meter bias was then added to the geoid field. The error of estimation for this set of anomalies ( $\hat{\Delta g}$ ) is shown in Table 7. Addition of the one meter bias increased the mean error from 0.2 mgal to 1.5 mgal and the RMS from 2.9 mgal to 3.5 mgal.

Tests for the effects of random error in the geoid field were extended to include random errors with  $\sigma = 0.3, 0.6, 1.2$ , and

Table 6  
 ERROR OF ESTIMATION ( $\hat{\Delta g} - \overline{\Delta g}$ ) FOR  $1^\circ \times 1^\circ$  MEAN VALUES  
 FROM A GEOID WITH A RANDOM ERROR OF ONE METER

15.9	- 9.3	-16.9	-26.3	17.7	- 9.3	- 3.1	-11.7	-12.2	- 6.3
- 7.5	6.9	2.6	-11.0	-21.7	- 3.8	- 2.8	0	7.6	- 8.3
- 0.7	- 0.6	5.6	- 7.4	16.5	-10.3	- 4.6	0.5	14.8	4.5
2.9	4.2	3.9	- 1.2	- 3.9	- 1.1	-12.9	-11.7	15.1	- 1.3
- 4.5	16.3	- 1.8	- 0.5	6.1	13.9	-11.7	8.4	- 6.6	- 2.8
4.0	11.4	2.9	3.7	1.9	-14.2	4.1	2.2	- 2.5	9.3
- 5.6	1.3	- 0.3	4.7	- 5.0	3.3	3.8	21.2	0.9	5.4
22.7	14.1	7.9	6.2	- 2.4	0.6	7.6	- 8.7	10.0	- 4.7
0.8	4.7	5.3	- 5.3	-12.6	-10.9	3.6	- 8.0	- 6.4	5.9
- 5.2	- 1.9	- 1.2	- 4.7	18.1	5.3	- 3.2	- 6.2	- 1.6	- 4.7

5° x 5° INTEGRATION

MEAN VALUE = 0.1 mgal

RMS = 9.0 mgal

Table 7  
 ERROR OF ESTIMATION ( $\hat{\Delta g} - \overline{\Delta g}$ ) FOR  $1^\circ \times 1^\circ$  MEAN VALUES  
 FROM A GEOID WITH A BIAS ERROR OF ONE METER

- 2.2	0.7	3.0	2.7	2.0	- 1.4	6.8	3.5	0.9	- 0.5
- 1.8	- 1.0	1.6	3.2	2.7	2.5	3.4	2.4	- 1.0	- 3.7
1.3	3.3	- 1.0	2.8	2.9	1.2	1.1	0.3	- 3.2	- 1.7
- 2.5	- 5.5	- 3.5	1.5	1.8	- 0.9	- 1.3	- 0.9	- 2.0	- 3.3
- 1.5	- 7.4	- 6.4	- 0.2	1.0	- 1.6	- 1.1	1.4	2.7	1.6
- 0.3	- 7.6	- 8.8	- 3.4	- 2.0	- 3.6	- 3.1	- 0.5	1.6	- 1.5
- 6.8	- 5.1	- 8.2	- 4.1	- 3.2	- 4.9	- 5.5	- 4.7	- 3.5	- 3.5
- 8.2	-11.2	- 8.1	- 3.8	- 1.9	- 2.2	- 2.0	- 1.1	- 0.9	- 2.1
- 4.9	- 6.0	- 3.6	- 1.5	0	1.6	2.1	1.5	1.1	- 0.5
- 0.7	- 3.7	- 0.4	- 1.4	- 1.8	- 1.5	- 2.0	- 3.0	- 2.9	- 2.8

$5^\circ \times 5^\circ$  INTEGRATION

MEAN VALUE = -1.5 mgal

RMS = 3.5 mgal



3.0 meters, all with zero mean. The error of estimation increased from 2.9 mgal to 26.2 mgal as  $\sigma$  increased from 0 to 3 meters. Results of this analysis are shown in Figure 15. Also shown are results for 2.5° and 5° elements accomplished by averaging the 1° results, and, as expected, the error is reduced as the element size is increased.

For the purpose of iterative improvement, new geoid heights were computed from the estimated anomalies by Stokes' integral and a  $\Delta N$  field was obtained by subtracting the true geoid heights from the new geoid heights. The  $\Delta N$  values were input to the estimation program and corrections to the original anomaly estimates were computed with an algebraic solution over a 5° x 5° integration region. The corrected estimates are compared with point and mean anomalies in Table 8.

Table 8  
ITERATIVE IMPROVEMENT  
(36 1° x 1° SQUARES)

RMS	MEAN ANOMALIES	POINT ANOMALIES
First Estimate	2.20 mgal	4.42 mgal
Iteration	1.45 mgal	2.23 mgal

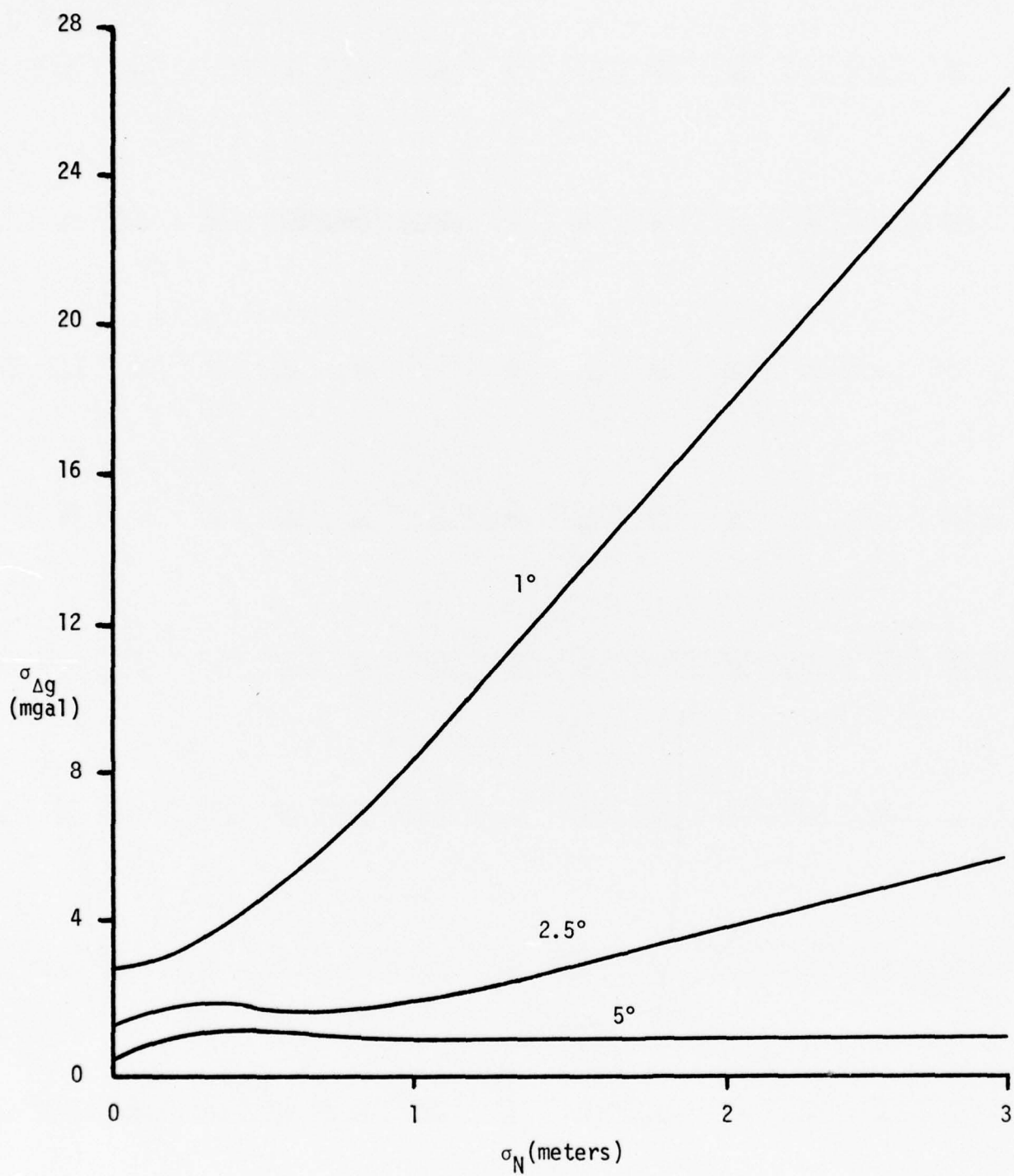


Figure 15. Effects of Random Error on Gravity Anomalies.

## VII. CONCLUSIONS

It is possible to localize the estimation of gravity anomalies from a  $1^\circ \times 1^\circ$  gridded data base of geoid height values. The method of localization consists of:

Approximating the low degree (long wave length) component of gravity anomalies and geoid heights from the harmonic coefficients of an earth gravitational model.

Estimating the high degree (short wave length) components of gravity anomalies from high degree components of geoid heights over a local region with a linear estimator.

Mean gravity anomalies for  $1^\circ \times 1^\circ$  squares can be effectively estimated from localized geoid heights which contain random errors whose standard deviation is one meter or less. Random errors with a standard deviation of three meters increase the RMS error of estimation to 26 mgal. Mean anomalies for  $5^\circ \times 5^\circ$  squares can be locally estimated from  $1^\circ \times 1^\circ$  geoid heights whose random errors have a standard deviation as large as three meters. A bias of one meter in the local geoid height field, if not removed, has a significant effect on the mean error of the gravity anomaly estimates, although such a bias does not change the RMS error of estimation appreciably.

Errors in the low degree harmonic coefficients of the EGM affect both the high and low degree components of the anomaly estimates. These errors can be reduced by updating the EGM as altimetry data accumulates. Methods of avoiding the singularity of



Stokes' kernel function, the use of smaller element sizes and methods of minimizing the effects of bias in the data are indicated to be areas for further study.

The unweighted least squares estimator is not necessarily the best choice of estimation model since it does not use all available data. The model could be modified to use weight matrices derived from covariance matrices and to compute corrections for initial estimates of gravity anomalies. Moreover, the selected estimator apparently does not achieve the optimum resolution of the data into signal (true values) and noise (random errors). Additional study is also indicated in this area.



## APPENDIX

### PREDICTION OF GEOID HEIGHTS FROM PROFILE DATA

#### A1. INTRODUCTION

Profile data for GEOS-III altimetry consists of measured geoid heights at closely spaced intervals along approximately parallel tracks. This appendix outlines a method for estimating the prediction error covariance function for Wiener prediction of a geoid height gridded data base from profile data. The error covariance function is computed in the frequency domain for simplicity since integrations in the time domain become multiplications in the frequency domain. The accuracy of the predicted  $1^\circ \times 1^\circ$  geoid height values is given by the error integral, which is the integral of the error covariance function over the  $1^\circ \times 1^\circ$  surface elements. Also included in the discussion are geoid height autocovariance, power spectra, geoid height prediction, the spectral coefficients of the Wiener equation and their application in the error analysis of predicted geoid heights.

#### A2. THE GEOID HEIGHT AUTOCOVARANCE FUNCTION

The prediction method is based on the assumption that the geoid height field can be treated as an isotropic stationary stochastic process. The effect of isotropy for a covariance function between two profiles with an origin at point P is shown in Figure A1. The value of the geoid height autocovariance function relating points P and Q depends only on the angular distance between P and Q and not

on the location of the points or the direction of one from the other.  
The line segment  $PQ'$  is normal to both profiles.

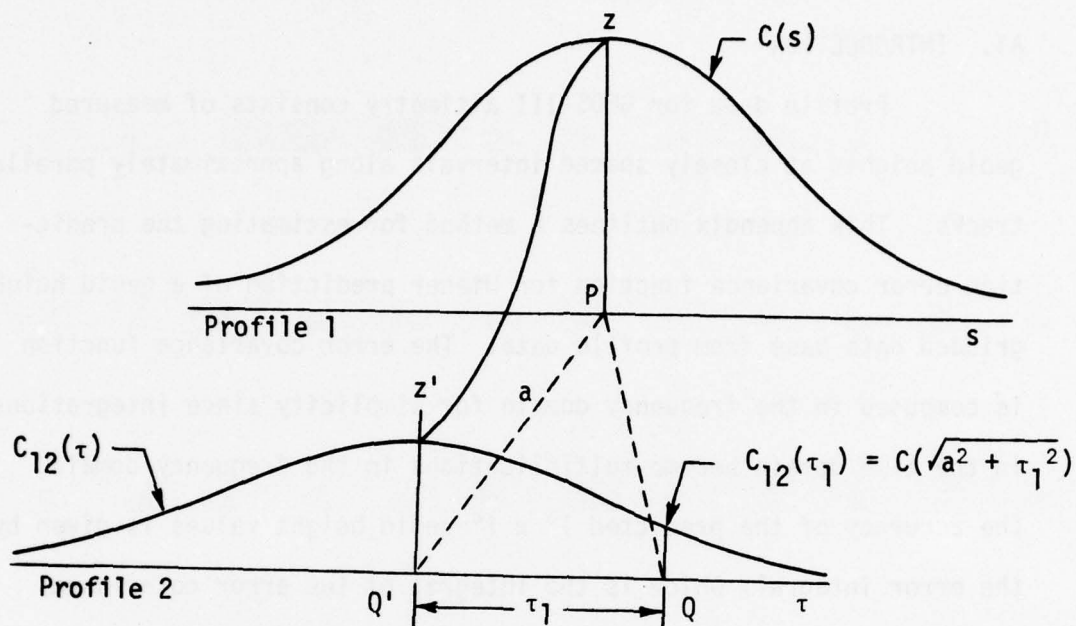


Figure A1. Geoid Height Autocovariance Function

In these computations, a form of the geoid height autocovariance function of Tscherning and Rapp [4], with the low degree and the high degree parts removed, is used:

$$C(\psi) = \frac{R^2}{\gamma^2} \sum_{n=13}^{1080} \frac{C_n}{(n-1)^2} F^{n+1} P_n(\cos \psi), \quad (A1)$$

where

$R$  = Mean radius of earth,

$\gamma$  = Theoretical gravity of the reference ellipsoid,

$P_n(\cos \psi)$  = Legendre polynomial of degree  $n$ ,

$\psi = \sqrt{a^2 + \tau_1^2}$ , Spherical distance between  $P$  and  $Q$ ,

$$C_n = \frac{A(n-1)}{(n-2)(n+B)} \text{ degree variance of degree } n, \text{ where}$$

$$A = 425.28 \text{ mgal}^2,$$

$$B = 24,$$

$$F = \frac{R_B^2}{r_P r_Q} = 0.999617,$$

$$R_B = \text{Radius of the Bjerhammar sphere,}$$

$$r_P \text{ and } r_Q = \text{Geocentric radii to the points P and Q.}$$

### A3. POWER SPECTRA

#### 1. The Power Spectrum Along a Profile

Assuming the statistics of the local field are known, the power spectrum for observations along a profile can be determined by the Fourier Transform of the geoid height covariance function. Thus, the power spectrum is

$$S(\omega) = \int_{-\infty}^{\infty} C(s) e^{-i\omega s} ds. \quad (A2)$$

Since

$$e^{-i\omega s} = \cos(\omega s) - i \sin(\omega s),$$

the power spectrum can be expressed as

$$S(\omega) = \int_{-\infty}^{\infty} C(s) \cos(\omega s) ds - i \int_{-\infty}^{\infty} C(s) \sin(\omega s) ds, \quad (A3)$$

and since  $C(s)$  is an even function,

$$\int_{-\infty}^{\infty} C(s) \sin(\omega s) ds = 0, \quad (A4)$$

so that the expression for the spectrum reduces to

$$S(\omega) = \int_{-\infty}^{\infty} C(s) \cos(\omega s) ds. \quad (A5)$$

Since  $C(s)$  is symmetric, the continuous power spectrum along a profile reduces to

$$S(\omega) = 2 \int_0^{\infty} C(s) \cos(\omega s) ds, \quad (A6)$$

which can also be expressed in discrete form as

$$S(r\Delta\omega) = \Delta s [C(0) + 2 \sum_{q=1}^{n-1} C(q\Delta s) \cos(\frac{rq\pi}{n}) + C(n\Delta s) \cos(r\pi)], \quad (A7)$$

where  $n$  equally spaced values of the covariance function are used,

$$r = 0, 1, 2, \dots, n,$$

$$\Delta\omega = \frac{\pi}{n\Delta s}.$$

The notation for the various power spectra to be used is  $S_{ij}(\omega)$  for the spectral value between points on profiles  $i$  and  $j$  for frequency  $\omega$ , and it is assumed the along track spectrum is identical for all profiles in a local area ( $i = j$ ), or

$$S_{11}(\omega) = S_{22}(\omega) = S_{33}(\omega). \quad (A8)$$

## 2. The Across Track Power Spectrum

The spectrum  $S_{12}(\omega)$  of the covariance function  $C_{12}(\tau)$  between points on two adjacent profiles is also the Fourier transform of the covariance function

$$S_{12}(\omega) = \int_{-\infty}^{\infty} C_{12}(\tau) e^{-i\omega\tau} d\tau. \quad (A9)$$



Again, since  $C_{12}(\tau)$  is an even function of  $\tau$ ,

$$S_{12}(\omega) = 2 \int_0^{\infty} C_{12}(\tau) \cos(\omega\tau) d\tau. \quad (A10)$$

From Figure A1, if  $a$  is the separation between the profiles, then

$$C_{12}(\tau) = C(\sqrt{a^2 + \tau^2}), \quad (A11)$$

so that the crosstrack spectrum is

$$S_{12}(\omega) = 2 \int_0^{\infty} C(\sqrt{a^2 + \tau^2}) \cos(\omega\tau) d\tau. \quad (A12)$$

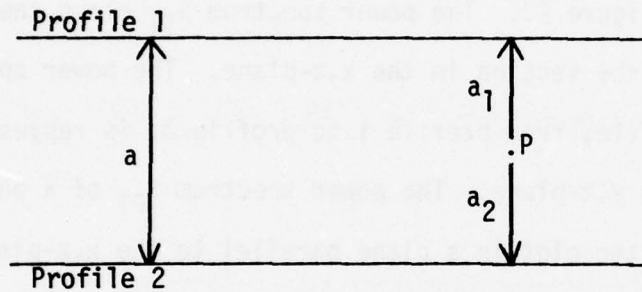


Figure A2. Geometry of Profiles

Similarly, the power spectrum  $S_{p1}(\omega)$  between the point P and profile 1, Figure A2 is

$$S_{p1}(\omega) = 2 \int_0^{\infty} C(\sqrt{a_1^2 + \tau^2}) \cos(\omega\tau) d\tau. \quad (A13)$$

The discrete form for equation (A12) is

$$S(r\Delta\omega) = \Delta s [C_{12}(0) + 2 \sum_{q=1}^{n-1} C_{12}(q\Delta\tau) \cos(\frac{qr\pi}{n}) + C_{12}(n\Delta\tau) \cos(r\pi)], \quad (A14)$$

where

$$C_{12}(q\Delta\tau) = C(\sqrt{a_1^2 + (q\Delta\tau)^2}),$$

$$r = 0, 1, 2, \dots, n,$$

$$q = 0, 1, 2, \dots, n.$$

The transformation of the data from the distance domain to the frequency domain is followed by a smoothing process to reduce spectral leakage and aliasing [8].

The power spectrum computed from equations (A7) and (A14) is plotted in Figure A3. The power spectrum  $S_{11}$  along the profile is represented by the section in the  $x,z$ -plane. The power spectrum  $S_{13}$  across the profile, from profile 1 to profile 3, is represented by the plot in the  $y,z$ -plane. The power spectrum  $S_{p1}$  of a point P is represented by the plot in a plane parallel to the  $x,z$ -plane at some distance along the  $y$ -axis.

#### A4. GEOID HEIGHT PREDICTION

##### 1. The Fundamental Equation for Prediction

The predicted geoid height  $y_p$  is assumed to be a linear function of the measured values  $x_i$  so that the fundamental equation for prediction [3] along one profile is

$$y_p(\tau) = \int_{-\infty}^{\infty} h_p(\tau - \alpha) x(\alpha) d\alpha. \quad (A15)$$

The coefficients  $h_p$  depend on the displacements of the measurements relative to point P, not their magnitudes. The prediction of the

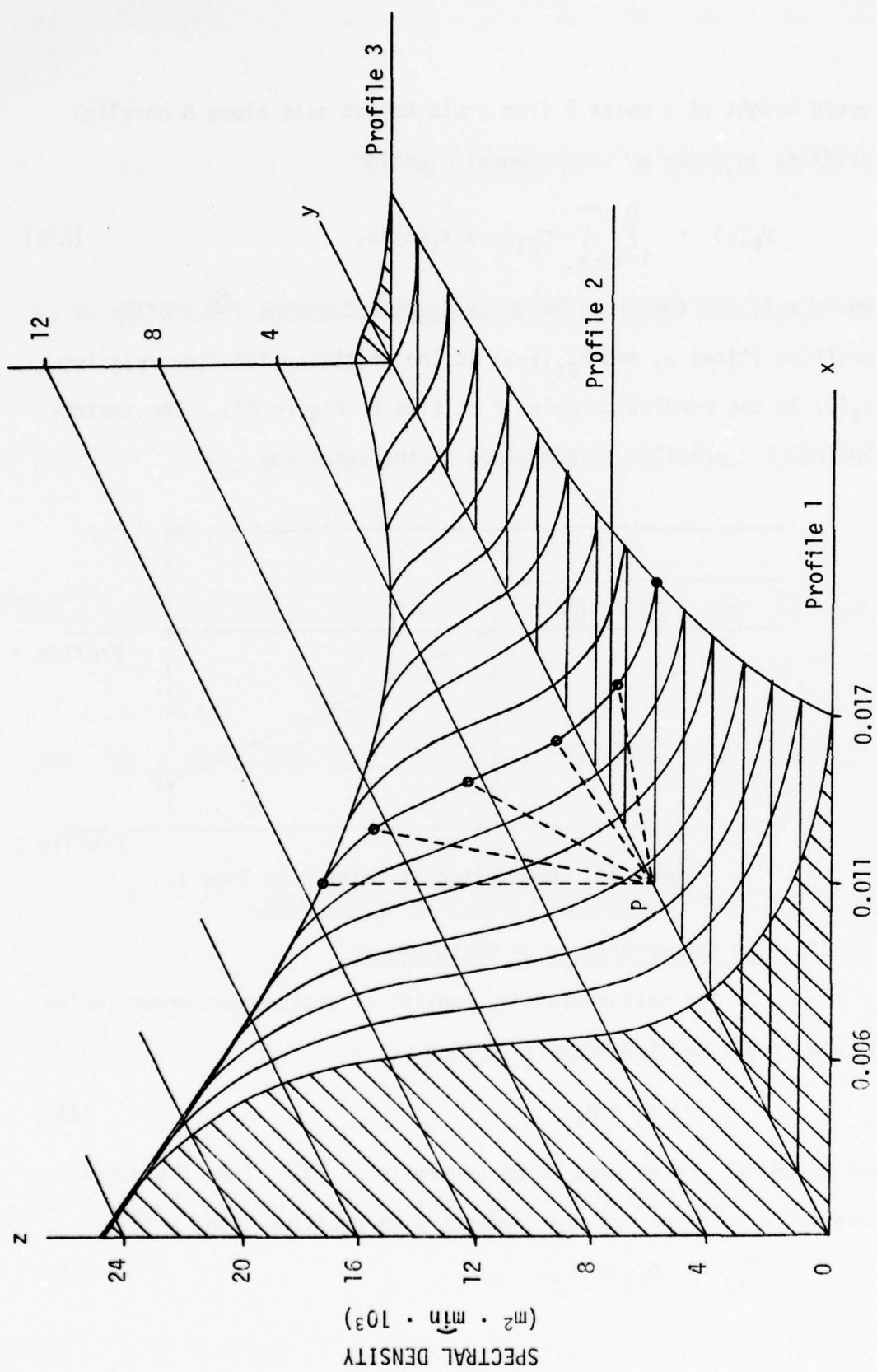


Figure A3. Power Spectrum of Geoid Heights.

geoid height at a point P from geoid height data along n parallel profiles is given by the integral equation

$$y_p(\tau) = \sum_{i=1}^n \int_{-\infty}^{+\infty} h_{pi}(\tau-\alpha) x_i(\alpha) d\alpha, \quad (A16)$$

where  $x_i(\alpha)$  is the geoid height measurement on the  $i^{\text{th}}$  profile at position (time)  $\alpha$ , and  $h_{pi}(\tau-\alpha)$  is the weighting function relating  $x_i(\alpha)$  to the prediction point P at time  $\tau$  (Figure A4). The contribution of n profiles is contained in the summation.

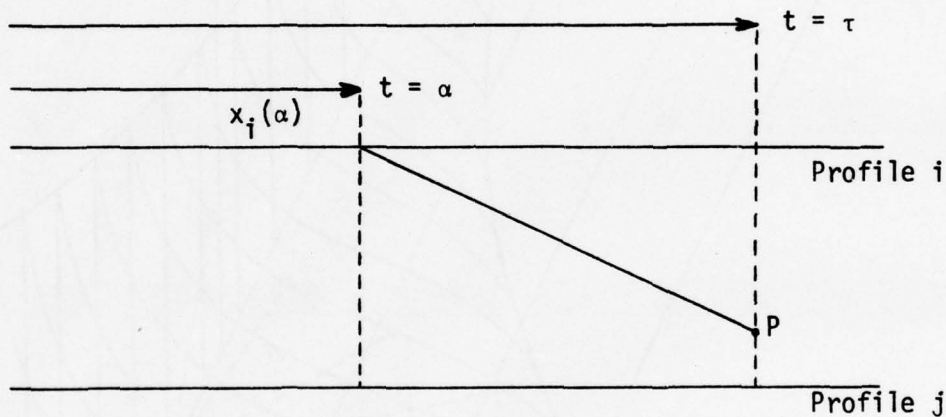


Figure A4. Prediction of Point P at Time  $\tau$ .

## 2. The Autocovariance of Measurements

The measurements  $x_i$  consist of measurement error (noise)  $n_i$  and true value (signal)  $s_i$  so that

$$x_i = s_i + n_i, \quad (A17)$$

and  $n_i$  and  $s_i$  are assumed to be uncorrelated [3]. Then the autocovariance function for measurements  $x$  on profiles  $i$  and  $j$  is

$$\bar{C}_{ij} = C_{ij} + D_{ij}, \quad (A18)$$



where

$\bar{C}_{ij}$  = the autocovariance of observations  $x_i, x_j$ ,

$C_{ij}$  = the autocovariance of the signal  $s_i, s_j$ ,

$D_{ij}$  = the autocovariance of noise  $n_i, n_j$ .

### 3. System Functions for Optimal Prediction

In this section, the Wiener-Hopf equation is solved for the system functions whose inverse Fourier transforms are the weighting functions for an optimal prediction by equation (A16). The geometry for prediction from two profiles is shown in Figure A5.

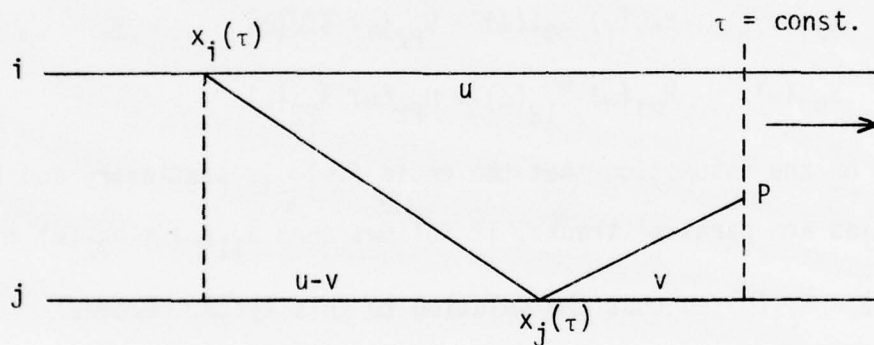


Figure A5. Combined Filtering and Prediction.

The Wiener-Hopf system of linear equations is

$$\sum_{i=1}^n \int_{-\infty}^{\infty} h_{pi}(u) \bar{C}_{ij}(u-v) du = C_{pj}(v), \quad j = 1, 2, \dots, n \quad (A19a)$$

or in the compact convolution notation

$$\sum_{i=1}^n h_{pi}(v) * \bar{C}_{ij}(v) = C_{pj}(v), \quad j = 1, 2, \dots, n. \quad (A19b)$$

Its spectral representation is

$$\sum_{i=1}^n H_{pi}(\omega) \bar{S}_{ij}(\omega) = S_{pj}(\omega), j = 1, 2, \dots n \quad (A20)$$

which can easily be solved for the system functions  $H_{pi}(\omega)$ , provided the spectrums of the covariance functions are known (Section A5). A sample weighting function in the frequency domain as a function of distance from profile 1 is shown in Figure A6.

#### A5. SYSTEM FUNCTIONS FOR THE TWO PROFILE CASE

For prediction at point P between two profiles (Figure A5), the Wiener-Hopf equation (A20) in the frequency domain expands to

$$S_{p1}(\omega) = H_{p1}(\omega) \bar{S}_{11}(\omega) + H_{p2}(\omega) \bar{S}_{21}(\omega), \quad (A21)$$

$$S_{p2}(\omega) = H_{p1}(\omega) \bar{S}_{12}(\omega) + H_{p2}(\omega) \bar{S}_{22}(\omega). \quad (A22)$$

Based on the assumption that the geoid field is stationary and the profiles are parallel tracks, it follows that  $\bar{S}_{11}(\omega) = \bar{S}_{22}(\omega)$  and  $\bar{S}_{12}(\omega) = \bar{S}_{21}(\omega)$  so that the solution to this system becomes:

$$H_{p1}(\omega) = \frac{S_{11}(\omega) S_{p1}(\omega) - S_{12}(\omega) S_{p2}(\omega)}{\bar{S}_{11}(\omega)^2 - \bar{S}_{12}(\omega)^2}, \quad (A23)$$

and

$$H_{p2}(\omega) = \frac{\bar{S}_{11}(\omega) S_{p2}(\omega) - \bar{S}_{12}(\omega) S_{p1}(\omega)}{\bar{S}_{11}(\omega)^2 - \bar{S}_{12}(\omega)^2}, \quad (A24)$$

where

$H_{pi}(\omega)$  = the system weighting function for point P from profile i,

$\bar{S}_{11}(\omega)$  = the geoid height power spectrum along profile,

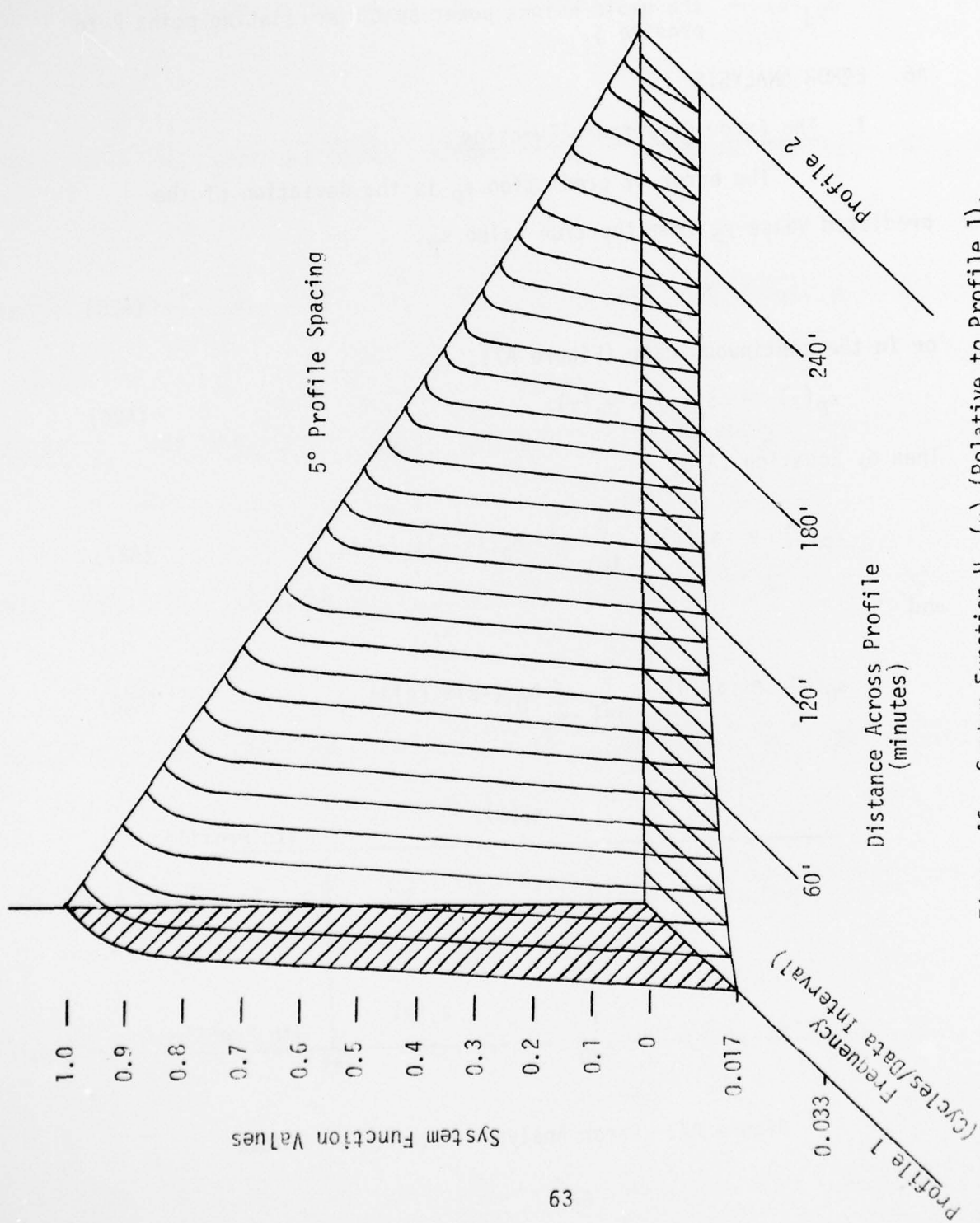


Figure A6. System Function  $H_{p1}(\omega)$  (Relative to Profile 1).

$\bar{S}_{12}(\omega)$  = the geoid height power spectrum across profile,

$S_{pj}(\omega)$  = the geoid height power spectrum relating point P to profile j.

#### A6. ERROR ANALYSIS

##### 1. The Error Covariance Function

The error of prediction  $\epsilon_p$  is the deviation of the predicted value  $y_p$  from the true value  $s_p$ ,

$$\epsilon_p = s_p - y_p, \quad (A25)$$

or in the continuous case (Figure A7),

$$\epsilon_p(\tau) = s_p(\tau) - y_p(\tau). \quad (A26)$$

Then by Equation (A16)

$$\epsilon_p(\tau) = s_p(\tau) - \sum_{i=1}^n \int_{-\infty}^{\infty} h_{pi}(\tau-\alpha) x_i(\alpha) d\alpha, \quad (A27)$$

and

$$\epsilon_Q(0) = s_Q(0) - \sum_{j=1}^n \int_{-\infty}^{\infty} h_{Qj}(-\beta) x_j(\beta) d\beta. \quad (A28)$$

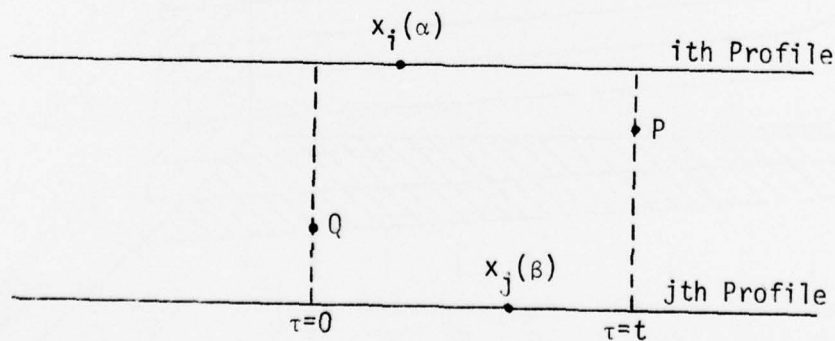


Figure A7. Error Analysis Between Two Points



The statistical mean,  $M$ , of the product  $\epsilon_P \epsilon_Q$  is the error covariance of prediction for points  $P$  and  $Q$ , and is denoted by  $\sigma_{PQ}$ .

$$\sigma_{PQ} = M\{\epsilon_P(\tau)\epsilon_Q(0)\}. \quad (A29)$$

Then,

$$\begin{aligned} \sigma_{PQ}(\tau) = & C_{PQ}(\tau) - \int_{-\infty}^{\infty} h_{Pi}(\tau-\alpha) C_{Qi}(-\alpha) d\alpha \\ & - \int_{-\infty}^{\infty} h_{Qj}(-\beta) C_{Pj}(\tau-\beta) d\beta \\ & + \int_{-\infty}^{\infty} \int_{-\infty}^{\infty} h_{Pi}(\tau-\alpha) h_{Qj}(-\beta) \bar{C}_{ij}(\alpha-\beta) d\alpha d\beta, \end{aligned} \quad (A30)$$

which is best solved by means of spectral representation [9]. The Fourier transform of equation (A30) is

$$\begin{aligned} E_{PQ}(\omega) = & S_{PQ}(\omega) - H_{Pi}(\omega) S_{Qi}(\omega) - H_{Qj}(\omega) S_{Pj}(\omega) \\ & + H_{Pi}(\omega) H_{Qj}(\omega) \bar{S}_{ij}(\omega). \end{aligned} \quad (A31)$$

After the weighting functions have been determined by the procedure outlined in Section A5, the error spectrum is easily computed with equation (A31). Then the error covariance function  $\sigma_{PQ}(\tau)$  is the inverse Fourier transform of  $E_{PQ}$ ; that is,

$$\sigma_{PQ}(\tau) = \frac{1}{2\pi} \int_{-\infty}^{\infty} E_{PQ}(\omega) e^{i\omega\tau} d\omega \quad (A32)$$

for different combinations of  $P$  and  $Q$ .

## 2. Error Variances for 1° x 1° Blocks

Assuming a sufficient distribution of predicted points, the variance of the geoid height for a 1° x 1° block is the mean

error covariance over all pairs of points  $P_i$  and  $P_j$  in the block;  
that is,

$$\sigma^2 = \frac{1}{n^2} \sum_{i=1}^n \sum_{j=1}^n \sigma_{ij}. \quad (\text{A33})$$

As an example with  $n = 9$ ,

$\sigma_{12}$  is the error covariance between point 1 (P)  
and 2 (Q)

$\sigma_{73}$  is the error covariance between point 7 (P)  
and point 3 (Q).

1	2	3
4	5	6
7	8	9

### 3. The Error Covariance Between $1^\circ \times 1^\circ$ Blocks

The error covariance between  $1^\circ \times 1^\circ$  blocks I and II is  
the mean covariance between all pairs of points  $P_i$  in I and  $Q_j$  in II;

I			II		
1	2	3	10	11	12
4	5	6	13	14	15
7	8	9	16	17	18

that is, for  $n = 9$

$$\sigma(I, II) = \frac{1}{n^2} \sum_{i=1}^9 \sum_{j=10}^{18} \sigma_{ij}. \quad (\text{A34})$$

### 4. The Error Integral

The error integral, often useful in studies of trajectory error or gravity survey requirements, is defined as

$$\frac{I(\phi, \lambda)}{R^2} = \int_A \int \sigma(\phi, \lambda, \phi', \lambda') \cos \phi' d\phi' d\lambda', \quad (\text{A35})$$

where A is the region of correlation, and  $\phi'$ ,  $\lambda'$  vary over A. For the discrete case using the error covariances defined above, this becomes

$$\frac{L(\phi_I, \lambda_I)}{R^2} = \sum_{II=1}^n \sigma(I, II) \cos \phi_{II} \Delta \phi_{II} \Delta \lambda_{II}. \quad (A36)$$

#### A7. COMPUTATIONAL RESULTS

Prediction error variances were computed for profile spacings of  $1^\circ$ ,  $2^\circ$ ,  $3^\circ 20'$  and  $5^\circ$ . Geoid height sigmas ( $\sigma_N$ ) of 0.0, 0.3, 0.6, 1.2 and 3.0 meters were used in each case. Error variances and error integrals in meters<sup>2</sup> for the  $1^\circ \times 1^\circ$  squares are shown in Tables A1 and A2, respectively. The error of prediction reaches its maximum value if the computation point is midway between two profiles. If  $\sigma_N = 3.0$  meters and the two profiles are spaced  $1^\circ$ ,  $2^\circ$ ,  $3^\circ 20'$  or  $5^\circ$  apart, then the maximum errors of prediction are 3.61, 3.85, 4.29 or 4.89 meters, respectively.

The computed error variances for prediction of geoid heights at points between profiles spaced  $1^\circ$ ,  $2^\circ$ ,  $3^\circ 20'$  and  $5^\circ$  apart are plotted in Figure A8. The total error variance for continuous prediction between profiles is the total area under the curve. The total error variance increases as the distance between profiles increases, although error variance for prediction near a profile decreases as the distance between input profiles increases.

Table A1  
Prediction Error Variances for 1° x 1° Squares  
(meters<sup>2</sup>)

Profile Spacing	Geoid Height Errors (one sigma)				
	0.0	0.3	0.6	1.2	3.0
1°	2.746	2.753	2.773	2.853	3.470
2°	3.528	3.537	3.563	3.666	4.446
	3.528	3.537	3.563	3.666	4.446
3°20'	3.444	3.453	3.477	3.577	4.328
	7.347	7.366	7.425	7.659	9.356
	5.400	5.414	5.455	5.620	6.832
	1.830	1.834	1.847	1.898	2.304
	6.694	6.711	6.764	6.975	8.509
5°	3.386	3.394	3.418	3.515	4.247
	8.800	8.823	8.894	9.179	11.229
	10.648	10.677	10.765	11.115	13.625
	8.800	8.823	8.894	9.179	11.229
	3.386	3.394	3.418	3.515	4.247



Table A2  
Error Integrals for 1° x 1° Squares  
(meters<sup>2</sup>)

Profile Spacing	Geoid Height Errors (one sigma)				
	0.0	0.3	0.6	1.2	3.0
1°					
	.001	.001	.001	.001	.001
2°					
	.005	.005	.005	.005	.006
	.005	.005	.005	.005	.006
3°20'					
	.011	.011	.011	.011	.014
	.021	.021	.021	.022	.022
	.016	.016	.016	.017	.020
	.007	.007	.007	.007	.009
	.020	.020	.020	.020	.025
5°					
	.013	.013	.014	.014	.017
	.037	.037	.037	.039	.048
	.048	.048	.048	.050	.062
	.037	.037	.038	.039	.048
	.014	.014	.014	.014	.017

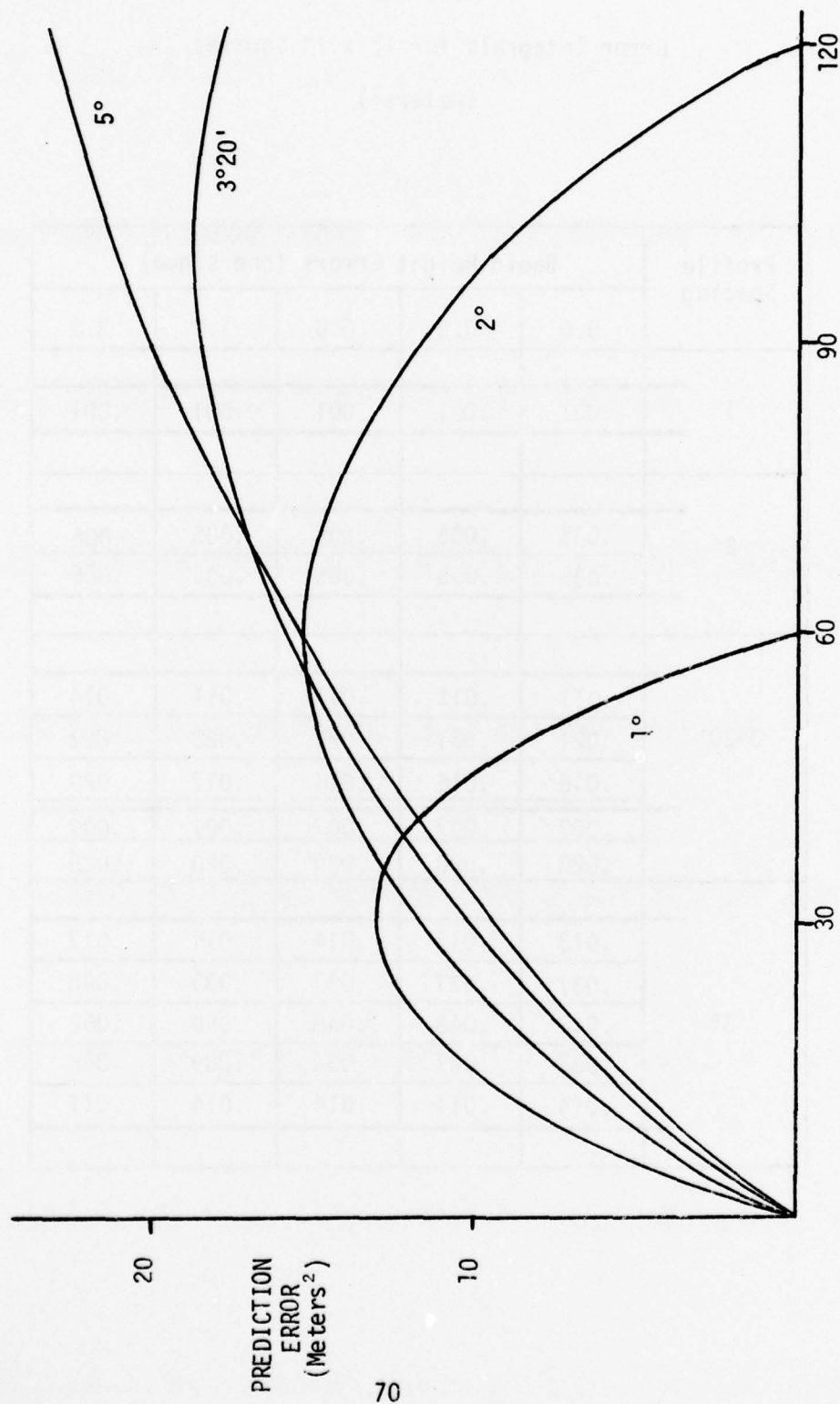


Figure A8. Distribution of Error Between the Profiles.

## REFERENCES

1. Defense Mapping Agency; DMA Plan for Exploitation of GEOS-C Observation Data; Washington, DC; 1974.
2. World Geodetic System Committee; The Department of Defense World Geodetic System 1972; May 1974 (Presented by Thomas O. Seppelin at the International Symposium on Problems Related to the Redefinition of North American Geodetic Networks, Fredericton, New Brunswick, Canada.)
3. Moritz, H.; A General Theory of Gravity Processing; AFCRL Report 69-0258; Report of the Department of Geodetic Science No. 122; The Ohio State University, Columbus, Ohio; 1969.
4. Tscherning, C.C. and R.H. Rapp; Closed Covariance Expressions for Gravity Anomalies, Geoid Undulations and Deflections of the Vertical Implied by Anomaly Degree Variance Models; AFCRL Report 74-0231; Report of the Department of Geodetic Science No. 208; The Ohio State University, Columbus, Ohio; 1974.
5. Heiskanen, W.A. and H. Moritz; Physical Geodesy; W.H. Freeman and Co.; San Francisco, California; 1967.
6. Moritz, H.; Advanced Least-Squares Methods; AFCRL Report 72-0363; Report of the Department of Geodetic Science No. 175; The Ohio State University, Columbus, Ohio; 1972.
7. Rapp, R.H.; Geopotential Coefficient Behavior to High Degree and Geoid Information by Wavelength; AFCRL Report 72-0506; Report of the Department of Geodetic Science No. 180; The Ohio State University, Columbus, Ohio; 1972.
8. Blackman, R.B. and Tukey, J.W.; The Measurement of Power Spectra; Dover Publications; New York, New York; 1959.
9. Papoulis, A.; Probability, Random Variables and Stochastic Processes; McGraw-Hill; New York, New York; 1965.

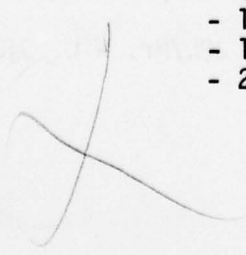
# Distribution List

Chief Scientist of AF	- 1	NSWC/DL	
		KA	- 2
USAF SAB	- 1	KR	- 2
Hq USAF		DIRSSPO	
IN	- 1	SP-23	- 1
AFIS/INTB	- 1	SP-24	- 1
RDQSM	- 1		
		USAETL/RI	- 1
CINCSAC			
IN	- 1	DARPA	- 1
INTSM	- 1		
JSTPS	- 1	DDC	-12
XPFR	- 1		
		ASD/XRT/DMAAC	- 3
AFSC			
SD	- 1	NASA	
DOXX	- 1	ES/Dr. J.W. Siry	- 1
IN	- 1	LRC/Mr. R.H. Tolson	- 1
		WFC/Mr. C.D. Leitao	- 1
SAMSO		GSFC/Mr. J.G. Marsh	- 1
MNNC	- 1	Dr. M.A. Kahn	- 1
IN/PWW	- 1	Mr. J.H. Berbert	- 1
SAMTEC/ROIS	- 1	NOAA	
		NGS/Mr. B.H. Chovitz	- 1
AFETR/DOSG	- 1	SOG/Dr. J.R. Apel	- 1
AFGL/LWG	- 2	C S Draper Lab/Mr. K. Fertig	- 1
RADC/IRRG	- 1	SAO/Dr. E.M. Gaposchkin	- 1
AU	- 1	OSU/Dr. R.H. Rapp	- 1
ADC	- 1	UCLA/Mr. W.M. Kaula	- 1
OOAMA/MME	- 1	LDGO/Dr. M. Talwani	- 1
USAFA		APL/JHU/Dr. H.D. Black	- 1
FJSRL	- 1		
DFACS	- 1	TASC/Dr. S.K. Jordan	- 1
AWC	- 1	JPL/Mr. W.L. Sjogren	- 1
NAVOCEANO	- 2		



# Distribution List (Cont'd)

Aerospace Corporation	
Mr. L. Wong	- 1
Observatoire de Parie	
Dr. K. Lambeck	- 1
Marine Sciences Directorate	
Mr. G.C. Dohler	- 1
University of New South Wales	
Dr. R.S. Mather	- 1
University of New Brunswick	
Department of Surveying	- 1
Engineering	
SAMSO/YED	- 6
DMA	
PR	- 1
ST	- 2
PPS	- 1
DMAHC/PR	- 2
DMATC (Code 52000)	- 2
DMATC/GSS	- 1
DMATC/Det 4, GSS	- 1
DMAAC	
PR	- 1
PRA	- 2
PRP	- 2
PRR	- 1
RDG	- 6
RDGG	- 2
RDGS	- 1
RDGT	- 2
RDGW	- 2
MDD	- 1
RDSL	- 1
RDN	- 2



UNCLASSIFIED

SECURITY CLASSIFICATION OF THIS PAGE (When Data Entered)

REPORT DOCUMENTATION PAGE		READ INSTRUCTIONS BEFORE COMPLETING FORM
1. REPORT NUMBER <b>14</b> DMAAC/TR-76- <b>001</b>	2. GOVT ACCESSION NO.	3. RECIPIENT'S CATALOG NUMBER
4. TITLE (and Subtitle) <b>6</b> RECOVERY OF GRAVITY ANOMALIES FROM GRIDDED GEOID HEIGHT DATA.	<b>9</b> FINAL	5. TYPE OF REPORT & PERIOD COVERED Technical Report, Final
7. AUTHOR(s) <b>10</b> Melvin E. / Shultz, Robert M. / Perlman, Joel B. / Starkey, James M. / Barth Daniel J. / Browning	8. CONTRACT OR GRANT NUMBER(s) iii	6. PERFORMING ORG. REPORT NUMBER
9. PERFORMING ORGANIZATION NAME AND ADDRESS Defense Mapping Agency Aerospace Center/RDG St. Louis AFS, MO 63118	10. PROGRAM ELEMENT, PROJECT, TASK AREA & WORK UNIT NUMBERS	
11. CONTROLLING OFFICE NAME AND ADDRESS Defense Mapping Agency Aerospace Center/PPC St. Louis AFS, MO 63118	12. REPORT DATE <b>11</b> JUL 1976	
14. MONITORING AGENCY NAME & ADDRESS (if different from Controlling Office)	13. NUMBER OF PAGES 71 <b>12</b> 794	15. SECURITY CLASS. (of this report) Unclassified
16. DISTRIBUTION STATEMENT (of this Report) Approved for Public Release, Distribution Unlimited		
17. DISTRIBUTION STATEMENT (of the abstract entered in Block 20, if different from Report)		
18. SUPPLEMENTARY NOTES		
19. KEY WORDS (Continue on reverse side if necessary and identify by block number) Satellite Altimetry      Geoid Heights GEOS-III      Satellite Geodesy Gravity Anomalies      Gravimetric Error Analysis		
20. ABSTRACT (Continue on reverse side if necessary and identify by block number) A gridded data base of geoid heights can be developed from GEOS-III satellite altimetry data. The derivation of two methods is discussed. A procedure for estimating gravity anomalies from the resulting geoid heights is described with simulations shown in tabular and graphic form. The report also discusses the computation of the calibration geoid for the GEOS-III test region, the data base from altimetry data and the simulation of test data for the estimation program. The method of		

DD FORM 1 JAN 73 1473

EDITION OF 1 NOV 65 IS OBSOLETE

UNCLASSIFIED

SECURITY CLASSIFICATION OF THIS PAGE (When Data Entered)

407789

UNCLASSIFIED

SECURITY CLASSIFICATION OF THIS PAGE(When Data Entered)

Block 20:

localization for estimation and the methods of testing the computer program are given in some detail. Test results which were computed from mid-1974 to early 1975 are included along with supporting tables and figures.

UNCLASSIFIED

SECURITY CLASSIFICATION OF THIS PAGE(When Data Entered)



END

FILMED

9-84

DTIC